The Astrophysical Journal, 689:622–645, 2008 December 10

IRON AND NICKEL ISOTOPIC RATIOS IN PRESOLAR SiC GRAINS

Kuljeet K. Marhas,[1,2] Sachiko Amari,[1] Frank Gyngard,[1] Ernst Zinner,[1] and Roberto Gallino[3,4]
Received 2008 May 28; accepted 2008 August 14

ABSTRACT

We report the first Fe isotopic anomalies and the first Ni isotopic ratio measurements in presolar SiC grains of separate KJG from the Murchison meteorite. With NanoSIMS, we analyzed Fe and Ni in 37 X grains from Type II supernovae and 53 SiC grains of other types. The Ni/Fe and Co/Fe ratios in grains of all types are much higher than in the gas from which the grains are believed to have condensed. A majority of the X grains and a couple of mainstream grains contain Fe-rich subgrains. Most X grains have large excesses in ^{57}Fe, ^{61}Ni, and ^{62}Ni. ^{60}Ni excesses are small and the ^{54}Fe/^{56}Fe ratios of almost all X grains are normal. These isotopic compositions are best explained by mixing of material from the He/N zone of Type II supernovae with material from the He/C zone. The lack of any ^{54}Fe excesses is puzzling in view of the fact that the Si/S zone, whose contribution resulted in the ^{28}Si excesses in X grains, is very rich in ^{54}Fe. It has yet to be seen whether elemental fractionation between Si and Fe is an explanation. The ^{57}Fe deficits observed in a few X grains remain unexplained. In comparison to the X grains, fewer mainstream and AB grains have anomalies. Observed ^{62}Ni excesses in some mainstream grains are larger than predicted for AGB stars of solar metallicity and are not accompanied by corresponding ^{61}Ni excesses. A Y grain and a Z grain have excesses in ^{54}Fe and ^{62}Ni, but close to normal ^{57}Fe/^{56}Fe and ^{60,61}Ni/^{58}Ni ratios. These isotopic compositions are not expected for grains from low-metallicity AGB stars.

Subject headings: dust, extinction — nuclear reactions, nucleosynthesis, abundances — stars: AGB and post-AGB — supernovae: general

1. INTRODUCTION

Among all the different types of stardust (presolar) grains identified in primitive meteorites (e.g., Bernatowicz & Zinner 1997; Nittler 2003; Clayton & Nittler 2004; Lodders & Amari 2005; Zinner 2007), SiC has been studied in greatest detail. In particular, thousands of isotopic measurements have been made on individual grains by secondary ion mass spectrometry (SIMS) in the ion microprobe.

On the basis of their C, N, and Si isotopic compositions, SiC grains have been classified into different groups (Hoppe et al. 1994; Hoppe & Ott 1997; Zinner 2007). Mainstream grains (~93%) are identified to have an origin in low-mass (1–3 $M_\odot$) carbon-rich asymptotic giant branch (AGB) stars of solar metallicity during their thermally pulsing (TP) phase (Lugaro et al. 2003). Grains of type Y and Z (~1% each) are believed to come from AGB stars of lower-than-solar metallicity (Hoppe et al. 1997; Amari et al. 2001b; Zinner et al. 2006b). For grains of type AB (~3%–4% of presolar SiC), characterized by low ^{12}C/^{13}C ratios, J-type carbon stars and post-AGB stars, such as Sakurai's object, which undergo a very late thermal pulse have been proposed as stellar sources (Amari et al. 2001c). However, the details of the nucleosynthetic processes that would produce the isotopic signatures of these grains are still not well understood. Silicon carbide grains of type X (~1%) have mostly isotopically light C, heavy N, high inferred ^{26}Al/^{27}Al ratios (up to 0.6), and large ^{28}Si excesses (Nittler et al. 1995; Hoppe et al. 2000). These isotopic signatures, in conjunction with large ^{44}Ca excesses from the decay of ^{44}Ti ($T_{1/2} = 60$ yr; Nittler et al. 1996; Hoppe et al. 1996) and large ^{49}Ti excesses, possibly from the decay of ^{49}V ($T_{1/2} =$ 337 days; Hoppe & Besmehn 2002), show that these grains must have originated in the ejecta of Type II supernovae (SNeII). Finally, a few SiC grains have low ^{12}C/^{13}C and ^{14}N/^{15}N ratios, high inferred initial ^{26}Al/^{27}Al ratios, and large ^{30}Si excesses relative to solar system ratios, indicative of an origin in nova ejecta (Amari et al. 2001a), although a SNII origin is also possible for these grains (Nittler & Hoppe 2005).

Although isotopic analyses of trace elements such as Al-Mg and Ti have been made in many presolar SiC grains, measurements of the Fe isotopes have been scarce (Hoppe et al. 1998, 2000; Marhas et al. 2004) and none of the Ni isotopes have been made. Here we report Fe and Ni isotopic measurements in presolar SiC grains, mainly mainstream, AB, and X grains. Preliminary reports of some of the data have been presented by Marhas et al. (2007a, 2007b).

2. EXPERIMENTAL

The analyzed grains are from the Murchison SiC fraction KJG (Amari et al. 1994). Of the grains in this fraction, 90% have sizes between 1.8 and 3.7 μm (Zinner et al. 2007). Candidates for AB and X grains were obtained by direct ion imaging of ^{12}C, ^{13}C, ^{28}Si, and ^{30}Si grains, deposited on gold foil from liquid suspension, in the Cameca IMS 3f ion microprobe. These imaging analyses were made at low mass resolving power, similar to the direct imaging searches for X grains (Nittler et al. 1995). Candidates for X grains were selected on the basis of low ^{30}Si/^{28}Si ratios and those for AB grains were selected on the basis of low ^{12}C/^{13}C ratios. These candidate grains, as well as randomly selected additional grains, were subsequently measured for their major element compositions in a scanning electron microscope (SEM) equipped with an energy dispersive X-ray spectroscopy (EDS) system, in order to confirm that the grains were indeed SiC.

The C, N, Si, Fe, and Ni isotopic compositions of the grains were obtained in the Cameca NanoSIMS. The NanoSIMS (Stadermann

[1] Laboratory for Space Sciences and the Physics Department, Washington University, One Brookings Drive, St. Louis, MO 63130; ekz@wustl.edu.

[2] Current address: Planetary and Geoscience Division, Physical Research Laboratory, Ahmedabad, Gujarat, 380009, India.

[3] Dipartimento di Fisica Generale, Università di Torino, Via P. Giuria 1, I-10125 Torino, Italy.

[4] Center for Stellar and Planetary Astrophysics, School of Mathematical Sciences, Monash University, P.O. Box 28, Victoria 3800, Australia.

et al. 1999a, 1999b) is an ion microprobe with high sensitivity and high spatial resolution, which makes it the instrument of choice for the isotopic analysis of very small grains. These performance properties are achieved through several features. First, at high mass resolving power, necessary for the separation of molecular interferences from the atomic ion of interest, the secondary ion transmission is >30 times higher than that of the Cameca IMS 3f. Second, the NanoSIMS has miniaturized electron multipliers (Slodzian 2003), four of which can be moved along the focal plane of the secondary ions. This means that up to five ion signals can be measured simultaneously ("multidetection"). This increases the overall sensitivity for isotopic measurements. In addition, in multidetection any temporal change in the secondary ion signal, unavoidable during analysis of small grains, does not affect the measured isotopic ratios as it would if magnetic peak jumping and just one detector were employed. Third, the NanoSIMS features a very small primary beam size. For Cs^+ primary ions, beam diameters smaller than 50 nm have been achieved and a beam diameter of 100 nm is routine. The reason for this is that the primary ions are incident normal to the sample surface, along the same axis secondary ions are extracted. As a consequence, the immersion lens can be placed very close to the sample surface, resulting in a large demagnification of the primary beam diameter. This configuration also increases the secondary ion collection, further contributing to the overall sensitivity.

C, Si, and CN (for the N isotopes) were measured as negative secondary ions produced by bombardment with Cs^+ ions. These analyses were made in a mode combining multidetection with magnetic peak switching. In the first magnetic field step ^{12}C, ^{13}C, $^{12}C^{14}N$, $^{12}C^{15}N$, and ^{28}Si ions were counted in five electron multipliers. In two subsequent field steps ^{29}Si and ^{30}Si were counted in the 5th detector. For most AB grains and a few mainstream grains, we did not obtain N isotopic ratios. In this case the C and Si isotopes were measured in multidetection while the magnetic field was kept constant under nuclear magnetic resonance (NMR) control. Synthetic SiC and silicon nitride were used as standards.

The Fe and Ni isotopic analyses were made with positive secondary ions produced with an O^- primary beam. We used two different setups, one without Co and one including Co. In the setup without Co, we measured ^{28}Si, ^{52}Cr, ^{54}Fe, ^{57}Fe, and ^{62}Ni in the first magnetic field step, ^{56}Fe, ^{58}Ni, and ^{61}Ni with detectors 2–4 in the second step, and ^{60}Ni with detector 3 in the third field step. In the setup with ^{59}Co we measured ^{28}Si, ^{52}Cr, ^{54}Fe, ^{57}Fe, and ^{59}Co in the first magnetic field step, ^{56}Fe, ^{58}Ni, and ^{61}Ni with detectors 2–4 in the second step, and ^{60}Ni and ^{62}Ni with detectors 2 and 3 in the third field step. An Fe-Ni compound and NIST Silicate Glass Certified Reference Material SRM 610 (previously NBS 610 glass), which contains nominal concentrations of 500 parts per million (ppm) of Cr, Fe, Co, and Ni (e.g., Kane 1998), were used as isotopic standards and to determine the absolute concentrations of these elements in the grains.

In order to obtain elemental concentrations of Fe, Co, and Ni in ppm weight we measured $^{56}Fe^+/^{28}Si^+$, $^{59}Co^+/^{28}Si^+$, and $^{58}Ni^+/^{28}Si^+$ ratios in the NIST SRM 610 glass. We compared these ratios with the concentrations of 464, 403, and 443 ppm for Fe, Co, and Ni in this standard (Rocholl et al. 1997) to derive ion yields of these elements relative to Si. We obtain 2.33 for Fe, 1.02 for Co, and 0.596 for Ni. These are not very different from the yields of 2.63, 1.66, and 0.86 obtained by Hinton (1990) for low-energy secondary ions from the same standard. For his analysis Hinton assumed Fe, Co, and Ni concentrations of 458, 390, and 459 ppm. Our ion yields were applied to the ion ratios measured in the grains to obtain elemental concentrations of Fe, Co, and Ni.

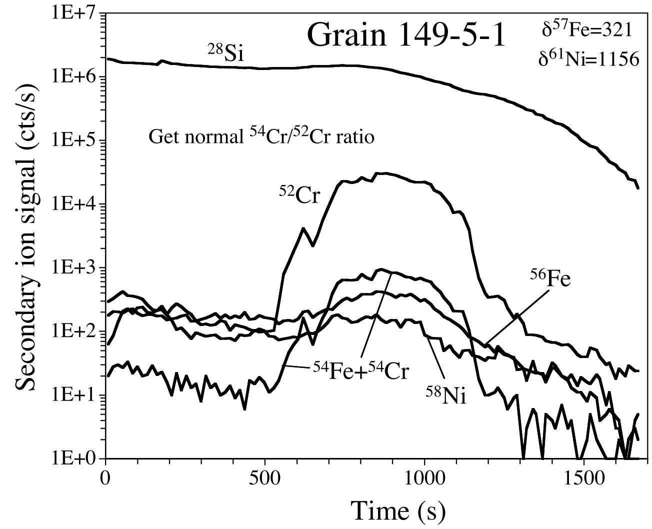

FIG. 1.—Secondary ion signals (in counts s^{-1}) of several isotopes measured during the analysis of X grain 149-5-1 plotted against the measurement time (in seconds). Because the primary O beam sputters away the grain layer by layer, the plot represents a depth profile of the grain's composition. During the measurement a Cr-rich subgrain was encountered. The ^{54}Cr signal dominates the ion signal at mass 54. If we assume a normal $^{54}Fe/^{56}Fe$ ratio, we obtain also a normal $^{54}Cr/^{52}Cr$ ratio for the Cr-rich subgrain.

Isotopic ratios of Fe and Ni are expressed relative to the most abundant isotopes ^{56}Fe and ^{58}Ni. The isobaric contributions of ^{54}Cr to ^{54}Fe and of ^{58}Fe to ^{58}Ni were corrected for by subtracting the calculated contributions of these interferences under the assumption of terrestrial (solar) $^{54}Cr/^{52}Cr$ and $^{58}Fe/^{56}Fe$ ratios. Typical corrections are a few percent for ^{54}Cr and a few permil (‰) for ^{58}Fe. The reason for the small ^{58}Fe interference is that Ni concentrations are high, in many grains higher than those of Fe (see below). In a few cases ^{54}Cr interferences are large (>100%), and in these cases the $^{54}Fe/^{56}Fe$ ratios should not be accepted with absolute confidence. An extreme case is X grain 149-5-1, where the inferred $^{54}Cr^+$ signal is 14 times as high as the inferred $^{54}Fe^+$ signal (see Fig. 1). In this case, we can invert this correction procedure and calculate the $^{54}Cr/^{52}Cr$ ratio by subtraction of ^{54}Fe and assuming a normal $^{54}Fe/^{56}Fe$ ratio. We thereby obtain a normal $^{54}Cr/^{52}Cr$ ratio. This grain has ^{57}Fe and ^{61}Ni excesses of 321‰ and 1156‰, respectively. If, as we shall argue below, these excesses are due to contributions from the He/C shell, we expect a corresponding ^{54}Cr excess between 300‰ and 600‰. Part of the Cr might have originated from contamination and would be isotopically normal; however, we do not know how much. Maximum ^{58}Fe interferences are 6% for grains 70-1 and 73-2. As will be seen and discussed in detail below, many X grains have excesses in ^{57}Fe ranging up to 1000‰. According to the most likely interpretation of these results in the framework of supernova models, ^{57}Fe excesses are expected to be accompanied by excesses in ^{54}Cr and ^{58}Fe. Thus, the $^{54}Fe/^{56}Fe$ ratios computed for such grains under the assumption of a normal $^{54}Cr/^{52}Cr$ ratio are strictly upper limits. Likewise, the $^{60,61,62}Ni/^{58}Ni$ ratios computed with normal $^{58}Fe/^{56}Fe$ ratios are strictly lower limits. However, it will be seen that, with assumed ^{54}Cr and ^{58}Fe excesses scaled to the ^{57}Fe excesses observed in the grains, the isotopic shifts are usually minor.

3. RESULTS

The elemental and isotopic data are given in Tables 1 and 2. Not all grains for which we obtained C and Si isotopic ratios had their Fe and Ni isotopes measured. Figures 2 and 3 show the N,

TABLE 1
Carbon, Nitrogen, and Silicon Isotopic Compositions of Presolar SiC Grains

Grain Type	Grain Number	$^{12}C/^{13}C$	$^{14}N/^{15}N$	$\delta^{29}Si/^{28}Si$ (‰)	$\delta^{30}Si/^{28}Si$ (‰)
X	57	243.4 ± 3.6	59.8 ± 0.9	−302 ± 5	−471 ± 4
X	77	143.1 ± 4.4	113.3 ± 3.1	−195 ± 7	−283 ± 8
X	80	48.1 ± 0.3	102.5 ± 1.5	−211 ± 3	−319 ± 7
X	97	508.6 ± 8.4	62.6 ± 0.7	−287 ± 4	−404 ± 4
X	115	396.9 ± 9.9	53.8 ± 0.6	−295 ± 4	−456 ± 8
X	226	648.5 ± 12.2	78.2 ± 1.3	−306 ± 5	−479 ± 10
X	422-1	199.3 ± 4.3	68.4 ± 1.0	−610 ± 4	−360 ± 7
X	432	570.0 ± 14.2	81.4 ± 1.5	−332 ± 4	−463 ± 5
X	446	143.0 ± 1.5	76.5 ± 1.3	−200 ± 6	−313 ± 5
X	424-2-1	230.4 ± 2.8	47.1 ± 0.8	−328 ± 6	−458 ± 4
X	69	1453.1 ± 36.9	43.7 ± 1.0	−303 ± 5	−438 ± 5
X	85	328.1 ± 4.7	87.8 ± 4.1	−287 ± 8	−481 ± 6
X	96	169.6 ± 2.1	154.0 ± 4.1	−598 ± 3	−523 ± 4
X	151	185.7 ± 1.3	63.6 ± 1.5	−295 ± 4	−432 ± 4
X	233	134.3 ± 1.1	37.8 ± 0.8	−228 ± 8	−410 ± 4
X	261	2234.3 ± 79.0	36.4 ± 0.8	−345 ± 5	−668 ± 4
X	287	136.7 ± 1.9	116.3 ± 4.1	−606 ± 4	−195 ± 7
X	337	2882.4 ± 77.0	21.0 ± 0.8	−366 ± 4	−705 ± 2
X	345	506.1 ± 12.2	65.1 ± 1.9	−291 ± 6	−417 ± 8
X	353	187.4 ± 2.4	91.8 ± 2.0	−276 ± 5	−379 ± 5
X	404	468.6 ± 5.1	76.4 ± 1.8	−312 ± 5	−441 ± 4
X	422-2	203.9 ± 2.1	63.5 ± 1.4	−151 ± 5	−264 ± 5
X	437	74.3 ± 0.4	207.4 ± 5.6	−685 ± 2	−520 ± 3
X	480	9455.1 ± 591.4	28.0 ± 0.7	−569 ± 3	−647 ± 2
X	482	1510.1 ± 29.8	45.3 ± 1.4	−480 ± 3	−363 ± 4
X	453-4	191.7 ± 2.1	64.3 ± 1.4	−267 ± 9	−498 ± 4
X	435-5	365.6 ± 3.8	64.4 ± 1.8	−314 ± 4	−520 ± 3
X	149-5-1	301.6 ± 3.2	99.0 ± 1.5	−267 ± 3	−417 ± 4
X	186-4	45.3 ± 0.3	67.5 ± 0.9	−180 ± 3	−269 ± 5
X	249-8	1128.8 ± 32.0	38.3 ± 0.5	−375 ± 3	−536 ± 5
X	293-1	136.7 ± 1.3	87.4 ± 1.0	−246 ± 3	−363 ± 4
X	339-1	39.5 ± 0.3	62.7 ± 1.1	−129 ± 4	−200 ± 6
X	443-6-2	678.5 ± 20.4	58.7 ± 0.7	−328 ± 4	−552 ± 5
X	444-2	147.3 ± 1.4	56.4 ± 1.1	−329 ± 3	−490 ± 3
X	532-1	85.9 ± 6.5	82.4 ± 2.5	−119 ± 3	−194 ± 5
X	557-1-2	189.6 ± 1.7	56.1 ± 0.6	−274 ± 3	−421 ± 5
X	66-1	164.8 ± 1.7	27.0 ± 0.4	−257 ± 6	−392 ± 4
X	70-1	116.7 ± 0.8	58.2 ± 0.8	−173 ± 8	−296 ± 7
X	73-2	159.0 ± 1.6	72.3 ± 0.8	−247 ± 4	−373 ± 4
X	82-1	344.6 ± 3.2	145.8 ± 2.6	−451 ± 4	−347 ± 5
M	1	43.9 ± 0.3	1375 ± 336	44 ± 15	40 ± 16
M	2	63.2 ± 0.6	459 ± 43	52 ± 5	54 ± 7
M	3	76.9 ± 0.6	1879 ± 203	38 ± 5	55 ± 6
M	5	40.8 ± 0.3	2315 ± 356	76 ± 5	76 ± 14
M	6	69.4 ± 0.7	524 ± 17	74 ± 12	62 ± 8
M	7	55.7 ± 0.4	536 ± 27	88 ± 12	72 ± 11
M	8	47.2 ± 0.4	1175 ± 85	60 ± 8	73 ± 7
M	9	54.0 ± 0.5	796 ± 60	54 ± 6	53 ± 8
M	10	64.9 ± 0.5	2755 ± 234	−9 ± 4	26 ± 10
M	70	49.2 ± 0.3	781 ± 124	30 ± 13	53 ± 16
M	406	45.7 ± 0.6	2455 ± 148	61 ± 5	50 ± 9
M	425	61.7 ± 0.6	3412 ± 289	48 ± 5	51 ± 7
M	466	92.4 ± 0.8	1388 ± 62	20 ± 4	47 ± 8
M	470	74.5 ± 0.7	884 ± 42	23 ± 6	31 ± 8
M	338-1	42.0 ± 0.4	2068 ± 145	171 ± 16	126 ± 18
M	422-3	53.3 ± 0.4	1499 ± 64	−4 ± 13	14 ± 11
M	424-2-2	51.0 ± 0.3	395 ± 20	97 ± 7	89 ± 7
M	424-4	73.8 ± 0.6	2251 ± 153	33 ± 5	53 ± 6
M	1-8-1	94.4 ± 0.6	2164 ± 107	−22 ± 6	−7 ± 7
M	1-8-2	66.3 ± 0.4	2323 ± 121	29 ± 6	34 ± 7
M	12	62.5 ± 0.4	1084 ± 85	55 ± 6	61 ± 7
M	14	46.5 ± 0.3	3441 ± 150	133 ± 7	112 ± 7
M	15	54.2 ± 0.4	1367 ± 137	2 ± 7	6 ± 13
M	18	47.5 ± 0.4	830 ± 58	67 ± 7	65 ± 8
M	19	63.1 ± 0.4	1198 ± 245	48 ± 9	46 ± 7

TABLE 1—*Continued*

Grain Type	Grain Number	$^{12}C/^{13}C$	$^{14}N/^{15}N$	$\delta^{29}Si/^{28}Si$ (‰)	$\delta^{30}Si/^{28}Si$ (‰)
M	20	68.2 ± 0.5	650 ± 74	40 ± 7	49 ± 7
M	21	65.7 ± 0.5	1849 ± 168	−1 ± 7	22 ± 7
M	22	52.6 ± 0.3	2081 ± 202	111 ± 9	89 ± 8
M	23	62.6 ± 0.6	374 ± 17	52 ± 7	55 ± 7
M	24	53.2 ± 0.3	2170 ± 153	24 ± 7	43 ± 10
M	109	91.7 ± 0.6	1463 ± 164	−8 ± 6	33 ± 7
M	118	73.3 ± 0.5	794 ± 81	18 ± 11	25 ± 10
M	121	92.2 ± 0.8	1437 ± 73	−3 ± 8	16 ± 7
M	340	52.8 ± 0.6	4069 ± 479	−10 ± 6	25 ± 11
M	482M	62.4 ± 0.3	1272 ± 57	56 ± 6	63 ± 7
M	2-11	52.6 ± 0.3	1424 ± 42	46 ± 4	53 ± 6
M	149-5	48.8 ± 0.3	1417 ± 76	97 ± 3	100 ± 7
M	195-5	61.3 ± 0.4	883 ± 34	58 ± 3	64 ± 6
M	195-5-1	39.2 ± 0.3	1456 ± 58	49 ± 4	52 ± 6
M	195-5-2	38.3 ± 0.3	794 ± 78	131 ± 4	129 ± 6
M	443-6	85.8 ± 0.6	515 ± 30	40 ± 4	61 ± 6
M	443-6-1	70.0 ± 0.5	1681 ± 103	24 ± 6	52 ± 8
M	557-1-1	43.8 ± 0.3	197 ± 21	103 ± 4	84 ± 7
M	8-5	62.7 ± 0.8	...	79 ± 17	56 ± 18
M	45-7	49.7 ± 0.5	...	59 ± 16	55 ± 16
M	135-7	43.3 ± 0.4	...	98 ± 16	93 ± 16
M	173-2	38.1 ± 0.4	...	88 ± 16	81 ± 17
M	174-10	50.7 ± 0.6	...	106 ± 17	95 ± 17
AB?	408	8.65 ± 0.05	2654 ± 279	−69 ± 5	−54 ± 12
AB	78	5.42 ± 0.03	3989 ± 574	56 ± 10	36 ± 11
AB	36-1	4.46 ± 0.05	...	62 ± 16	40 ± 16
AB	45-8	7.14 ± 0.07	...	−1 ± 15	33 ± 16
AB	49-8	4.53 ± 0.06	...	34 ± 14	16 ± 13
AB	86-1	5.75 ± 0.04	...	0 ± 12	25 ± 11
AB	89-2	7.79 ± 0.09	...	200 ± 14	151 ± 14
AB	109-2	5.16 ± 0.04	...	54 ± 12	26 ± 11
AB	115-3	4.45 ± 0.04	...	21 ± 12	86 ± 12
AB	119-2	4.59 ± 0.04	...	−38 ± 13	−25 ± 13
AB	123-7	3.20 ± 0.02	...	−19 ± 12	2 ± 11
AB	126-2	6.07 ± 0.04	...	−21 ± 12	24 ± 11
AB	132-4	2.89 ± 0.02	...	97 ± 13	67 ± 13
AB	132-8	2.51 ± 0.03	...	−49 ± 12	−43 ± 14
AB	135-8	2.07 ± 0.02	...	20 ± 16	32 ± 17
AB	141-2	5.32 ± 0.04	...	27 ± 12	19 ± 11
AB	144-2	2.88 ± 0.02	...	17 ± 13	20 ± 11
AB	173-1	5.35 ± 0.06	...	55 ± 16	26 ± 17
AB	174-11	3.14 ± 0.04	...	−6 ± 15	10 ± 15
AB	208-1	2.97 ± 0.02	...	85 ± 14	55 ± 13
AB	261-1	3.08 ± 0.02	...	−22 ± 11	0 ± 11
AB	309-4	4.83 ± 0.04	...	149 ± 14	108 ± 13
AB	333-3	6.08 ± 0.05	...	−27 ± 12	15 ± 11
AB	380-5	4.19 ± 0.03	...	73 ± 13	78 ± 12
AB	406-4	3.66 ± 0.04	...	−27 ± 12	−12 ± 11
Y	338-2	127.5 ± 1.5	693 ± 49	−42 ± 6	−3 ± 10
Y	4	115.1 ± 0.9	1667 ± 166	39 ± 4	90 ± 7
Y	16	141.2 ± 0.9	678 ± 40	−12 ± 6	44 ± 7
Y	284-1	109.1 ± 1.3	...	2 ± 12	26 ± 12
Z	17	60.7 ± 0.4	3258 ± 516	−136 ± 6	196 ± 8
Z?	557-1-2	32.8 ± 0.3	559 ± 53	−30 ± 4	17 ± 6

NOTE.—All errors are 1 σ.

C, and Si isotopic ratios of the grains of this study. The Si isotopic ratios in Figure 3 are plotted as δ-values, deviations from the solar ratios in permil (‰). All X grains have ^{15}N excesses relative to solar. We use the $^{14}N/^{15}N$ ratio of air (272) for solar, although the ratio of 435 measured in Jupiter's atmosphere might be more representative of the solar ratio (Owen et al. 2001). Most X grains have larger than solar $^{12}C/^{13}C$ ratios, reaching almost 10,000. In a Si three-isotope plot (Fig. 3), most X grains lie close to a line with slope 0.6. These grains were named X1 grains by Lin et al. (2002). The rest of the X grains plot below this line but do not follow a simple trend.

Figure 4 shows the Fe isotopic ratios of those grains that differ from solar by more than twice the experimental uncertainty in either one or both ratios. As are the Si ratios in Figure 3, the Fe isotopic ratios are plotted as δ-values. With few exceptions the $^{54}Fe/^{56}Fe$ ratios of most grains are normal. Among the exceptions

TABLE 2

Fe, Co, and Ni Contents and Fe and Ni Isotopic Ratios of Presolar SiC Grains

Grain Type	Grain Number	Fe (ppm)	Ni (ppm)	Co (ppm)	^{54}Cr corr[a] (%)	δ^{54}Fe/^{56}Fe (‰)	δ^{57}Fe/^{56}Fe (‰)	^{58}Fe corr[b] (‰)	δ^{60}Ni/^{58}Ni (‰)	δ^{61}Ni/^{58}Ni (‰)	δ^{62}Ni/^{58}Ni (‰)
X.............	57	231	1203	. . .	3.5	28 ± 98	98 ± 164	3.3	42 ± 39	47 ± 169	189 ± 96
X.............	77	251	872	. . .	6.5	21 ± 43	−3 ± 82	4.9	10 ± 22	−29 ± 96	75 ± 52
X.............	80	78	383	. . .	10.2	−3 ± 64	111 ± 112	3.5	33 ± 27	264 ± 134	−15 ± 59
X.............	97	919	1743	. . .	1.2	−5 ± 30	890 ± 82	9.1	−11 ± 21	380 ± 118	53 ± 49
X.............	115	382	1635	. . .	4.7	−69 ± 37	194 ± 82	4.0	9 ± 19	223 ± 100	91 ± 45
X.............	226	177	667	. . .	5.2	−43 ± 47	400 ± 85	4.6	18 ± 30	412 ± 156	23 ± 67
X.............	432	375	525	. . .	2.4	−24 ± 22	685 ± 58	12.3	14 ± 22	402 ± 120	82 ± 50
X.............	446	556	1186	. . .	4.7	33 ± 26	386 ± 64	8.1	18 ± 23	272 ± 117	125 ± 55
X.............	424-2-1	1034	2577	. . .	2.2	−5 ± 14	115 ± 55	6.9	−1 ± 13	151 ± 69	58 ± 28
X.............	69	1754	5403	210.3	1.2	−114 ± 19	−436 ± 23	5.6	89 ± 20	−36 ± 43	799 ± 50
X.............	85	134	711	3.5	8.3	−47 ± 35	−330 ± 47	3.2	26 ± 22	−234 ± 58	44 ± 43
X.............	96	297	2174	. . .	4.8	16 ± 117	76 ± 207	2.3	−63 ± 50	. . .	217 ± 141
X.............	151	1046	997	26.0	0.9	−1 ± 19	878 ± 62	18.0	−8 ± 18	1033 ± 80	311 ± 38
X.............	233	2854	3028	52.7	0.9	−34 ± 19	85 ± 38	16.2	17 ± 19	268 ± 60	100 ± 35
X.............	261	170	993	. . .	3.8	−12 ± 47	1 ± 75	2.9	−19 ± 29	. . .	−3 ± 61
X.............	287	226	1318	8.1	7.8	9 ± 34	−138 ± 51	2.9	−20 ± 20	. . .	19 ± 39
X.............	337	244	1574	. . .	3.3	60 ± 64	84 ± 106	2.7	15 ± 34	−9 ± 131	86 ± 78
X.............	345	149	791	8.8	5.2	22 ± 33	126 ± 60	3.2	23 ± 21	450 ± 80	113 ± 42
X.............	353	3560	2290	46.0	0.7	5 ± 21	477 ± 52	26.7	−26 ± 21	493 ± 86	104 ± 44
X.............	404	1209	835	29.9	2.1	2 ± 22	497 ± 54	24.9	−14 ± 22	178 ± 81	82 ± 47
X.............	422-2	1379	1496	40.4	0.8	−7 ± 19	583 ± 53	15.8	−30 ± 18	488 ± 63	206 ± 36
X.............	437	221	1192	. . .	2.6	−62 ± 37	245 ± 67	3.2	45 ± 28	315 ± 108	528 ± 74
X.............	480	249	1638	. . .	4.1	−73 ± 70	254 ± 139	2.6	−33 ± 37	. . .	95 ± 91
X.............	482	264	1591	11.6	3.2	134 ± 77	83 ± 127	2.9	−2 ± 35	−217 ± 117	50 ± 79
X.............	453-4	544	3345	66.7	7.3	59 ± 46	−170 ± 66	2.8	1 ± 24	43 ± 82	58 ± 50
X.............	435-5	4504	4550	. . .	0.6	−4 ± 33	1023 ± 77	17.0	−29 ± 33	1017 ± 206	268 ± 87
X.............	149-5-1	105	318	10.9	1413.4	67 ± 31	321 ± 71	5.7	30 ± 25	1156 ± 179	223 ± 60
X.............	186-4	22	116	2.9	16.2	283 ± 146	137 ± 213	3.2	0 ± 58	1425 ± 399	105 ± 145
X.............	249-8	86	110	10.1	4.0	150 ± 158	730 ± 249	13.5	344 ± 129	4607 ± 1130	1230 ± 392
X.............	293-1	298	208	28.6	0.9	56 ± 91	558 ± 100	24.7	−40 ± 54	1193 ± 356	−42 ± 126
X.............	339-1	17	18	0.4	43.3	−140 ± 80	471 ± 204	16.1	−27 ± 101	460 ± 522	−64 ± 237
X.............	443-6-2	42	255	15.7	10.8	−60 ± 99	839 ± 219	2.9	8 ± 45	1481 ± 316	160 ± 112
X.............	444-2	183	349	26.3	1.7	−90 ± 56	1042 ± 105	9.0	92 ± 33	2624 ± 316	936 ± 106
X.............	66-1	305	175	7.4	2.4	−14 ± 36	656 ± 65	29.9	30 ± 29	1053 ± 190	192 ± 69
X.............	70-1	534	160	6.7	3.5	12 ± 32	546 ± 56	57.4	−41 ± 26	598 ± 154	229 ± 68
X.............	73-2	1795	538	37.8	0.6	−18 ± 34	595 ± 55	57.3	−50 ± 22	1054 ± 160	190 ± 54
X.............	82-1	2644	1021	43.3	0.4	−36 ± 29	734 ± 57	44.5	−6 ± 17	1127 ± 137	199 ± 37
M.............	1	554	3063	. . .	3.6	4 ± 44	50 ± 86	3.1	4 ± 20	220 ± 101	296 ± 51
M.............	2	100	459	. . .	8.5	10 ± 30	42 ± 72	3.7	25 ± 20	114 ± 92	55 ± 44
M.............	3	296	1601	. . .	3.5	43 ± 54	74 ± 99	3.2	5 ± 23	−8 ± 99	72 ± 53
M.............	5	116	590	. . .	14.0	−51 ± 37	52 ± 82	3.4	73 ± 23	. . .	70 ± 51
M.............	6	411	2032	. . .	4.6	70 ± 54	8 ± 95	3.5	13 ± 23	−80 ± 96	−52 ± 50
M.............	7	300	1569	. . .	6.3	24 ± 52	−41 ± 91	3.3	13 ± 22	−27 ± 95	7 ± 49
M.............	8	369	2122	. . .	3.0	−2 ± 64	70 ± 115	3.0	−2 ± 26	. . .	−41 ± 57
M.............	9	447	2403	. . .	4.1	−16 ± 39	−37 ± 78	3.2	11 ± 19	−14 ± 81	16 ± 41
M.............	10	219	1017	. . .	10.3	−96 ± 36	−32 ± 74	3.7	56 ± 19	85 ± 86	116 ± 43
M.............	70	517	2873	. . .	4.2	−41 ± 52	−35 ± 94	3.1	−3 ± 22	−29 ± 97	86 ± 53
M.............	406	271	1376	. . .	4.3	−59 ± 50	−5 ± 93	3.4	−3 ± 23	−29 ± 97	45 ± 52
M.............	466	203	919	. . .	6.4	−49 ± 24	10 ± 64	3.8	39 ± 17	92 ± 79	127 ± 38
M.............	470	394	1987	. . .	185.3	−68 ± 88	−4 ± 89	3.4	22 ± 22	−52 ± 92	88 ± 51
M.............	338-1	485	2705	. . .	3.7	33 ± 61	25 ± 106	3.1	29 ± 25	. . .	30 ± 56
M.............	424-2-2	447	617	. . .	258.8	−28 ± 45	64 ± 61	12.4	27 ± 19	. . .	69 ± 43
M.............	424-4	329	1851	. . .	3.1	−29 ± 55	138 ± 106	3.1	27 ± 24	2 ± 103	80 ± 55
M.............	1-8-2	280	1140	. . .	5.1	−12 ± 39	63 ± 59	4.2	28 ± 28	57 ± 99	175 ± 63
M.............	12	72	316	1.8	9.2	−12 ± 29	−112 ± 44	3.9	7 ± 20	. . .	116 ± 39
M.............	14	171	717	5.1	2.8	68 ± 31	143 ± 47	4.1	−16 ± 19	−6 ± 49	65 ± 34
M.............	15	356	2329	. . .	1.9	34 ± 74	123 ± 130	2.6	72 ± 39	. . .	266 ± 99
M.............	18	1442	2087	18.5	1.4	20 ± 24	−33 ± 40	11.9	−15 ± 22	22 ± 69	407 ± 53
M.............	19	253	892	6.8	5.6	17 ± 30	23 ± 51	4.9	32 ± 22	61 ± 67	42 ± 41
M.............	20	117	519	2.2	17.5	−26 ± 26	67 ± 42	3.9	11 ± 19	48 ± 47	71 ± 32
M.............	21	1560	8808	. . .	1.9	−6 ± 87	213 ± 167	3.0	−49 ± 44	551 ± 256	305 ± 128
M.............	22	392	1350	10.0	2.7	87 ± 30	73 ± 50	5.0	−5 ± 21	26 ± 63	204 ± 44
M.............	23	387	2202	6.8	11.1	−76 ± 38	−218 ± 55	3.0	30 ± 23	4 ± 72	−14 ± 43
M.............	24	139	749	2.8	4.0	−35 ± 29	−179 ± 44	3.2	5 ± 20	−172 ± 50	−1 ± 36
M.............	109	151	688	4.2	3.8	−28 ± 28	21 ± 50	3.8	63 ± 21	174 ± 64	90 ± 39

TABLE 2—*Continued*

Grain Type	Grain Number	Fe (ppm)	Ni (ppm)	Co (ppm)	^{54}Cr corr[a] (%)	δ^{54}Fe/^{56}Fe (‰)	δ^{57}Fe/^{56}Fe (‰)	^{58}Fe corr[b] (‰)	δ^{60}Ni/^{58}Ni (‰)	δ^{61}Ni/^{58}Ni (‰)	δ^{62}Ni/^{58}Ni (‰)
M	117	199	1087	...	5.2	56 ± 46	34 ± 68	3.2	−19 ± 28	−85 ± 93	125 ± 63
M	118	255	1549	...	5.7	−54 ± 56	−156 ± 85	2.8	−37 ± 31	159 ± 137	295 ± 84
M	121	146	859	...	5.5	−57 ± 47	56 ± 78	2.9	−27 ± 28	154 ± 116	403 ± 78
M	340	289	1829	8.5	2.4	4 ± 47	−154 ± 73	2.7	32 ± 26	−166 ± 78	118 ± 55
M	2-11	24	27	0.5	24.2	135 ± 128	184 ± 219	15.5	167 ± 136	...	−248 ± 252
M	443-6-1	76	183	2.7	11.3	12 ± 48	9 ± 69	7.1	180 ± 34	659 ± 173	248 ± 77
M	45-7	49	211	0.8	1291.4	93 ± 78	−14 ± 109	4.0	−47 ± 42	−87 ± 140	−23 ± 88
M	135-7	100	528	1.7	8.4	−39 ± 60	94 ± 93	3.3	92 ± 35	−138 ± 101	159 ± 71
M	173-2	160	851	3.0	7.0	−22 ± 51	−135 ± 73	3.2	5 ± 25	−81 ± 91	−4 ± 55
M	174-10	99	521	1.6	13.3	101 ± 78	41 ± 124	3.3	26 ± 37	227 ± 163	−13 ± 82
A+B	78	894	2327	31.4	2.2	60 ± 29	101 ± 52	6.6	−27 ± 22	79 ± 73	222 ± 49
AB	45-8	269	1563	8.8	236.1	−48 ± 53	8 ± 80	3.0	69 ± 54	136 ± 114	12 ± 70
AB	123-7	270	1603	5.3	6.6	2 ± 65	−39 ± 89	2.9	21 ± 32	161 ± 115	−11 ± 63
AB	132-4	93	378	1.3	29.9	48 ± 48	18 ± 78	4.2	−2 ± 32	98 ± 114	−16 ± 64
AB	132-8	176	885	2.6	7.3	−56 ± 75	3 ± 113	3.4	29 ± 39	−81 ± 136	73 ± 86
AB	135-8	150	541	6.0	14.6	−59 ± 47	255 ± 85	4.8	105 ± 35	72 ± 116	5 ± 66
AB	144-2	288	1238	6.4	4.9	−66 ± 53	−66 ± 71	4.0	48 ± 32	34 ± 103	75 ± 63
AB	173-1	380	2669	15.8	6.3	65 ± 46	86 ± 67	2.4	68 ± 22	21 ± 71	11 ± 43
AB	174-11	649	1836	6.5	3.3	0 ± 34	−45 ± 43	6.1	34 ± 22	−30 ± 72	88 ± 47
AB	208-1	189	729	6.1	7.6	−18 ± 39	89 ± 57	4.5	54 ± 28	2 ± 79	124 ± 53
AB	261-1	96	444	1.9	8.9	51 ± 54	82 ± 79	3.7	5 ± 30	104 ± 106	123 ± 64
Y	4	142	741	...	15.1	7 ± 50	43 ± 90	3.3	22 ± 21	...	26 ± 47
Y	16	327	2012	6.1	72.8	403 ± 68	75 ± 75	2.8	−31 ± 23	−4 ± 78	404 ± 59
Z	17	254	1655	6.2	3.5	288 ± 57	116 ± 89	2.6	8 ± 26	70 ± 92	218 ± 60

NOTE.—All errors are 1 σ.
[a] Correction of the ^{54}Cr interference to ^{54}Fe, made under the assumption of a solar ^{54}Cr/^{52}Cr ratio, in percent of ^{54}Fe signal.
[b] Correction of the ^{58}Fe interference to ^{58}Ni, made under the assumption of a solar ^{58}Fe/^{56}Fe ratio, in permil of ^{58}Ni signal.

are ^{54}Fe excesses in a Y grain and a Z grain. In contrast, many grains show both excesses and deficits in ^{57}Fe. Most X grains have excesses ranging up to 1000‰, but four have deficits, including one grain with deficits in both ^{54}Fe and ^{57}Fe. Four mainstream grains also have ^{57}Fe deficits. Previously, Hoppe et al. (2000) measured ^{54}Fe/^{56}Fe ratios in eight X grains but found only normal ratios (within fairly large errors.) More precise NanoSIMS measurements of four mainstream, two AB, and one X grain gave also normal ^{54}Fe/^{56}Fe and ^{57}Fe/^{56}Fe ratios (Marhas et al.

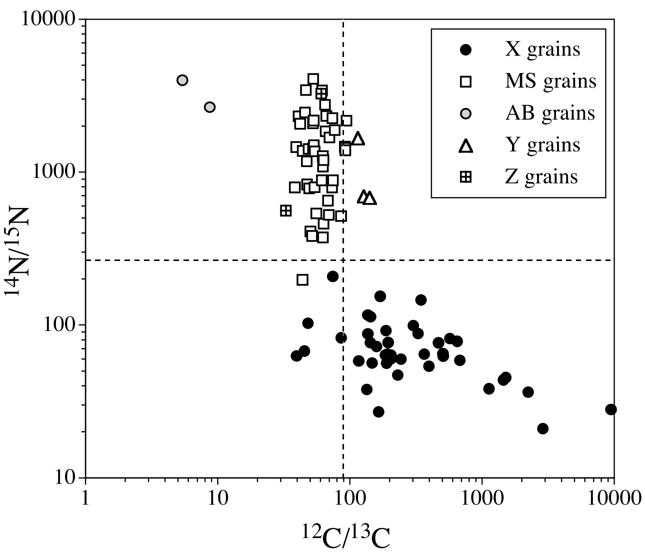

FIG. 2.—N and C isotopic ratios of grains of this study. N isotopic ratios were not measured in all grains (see Table 1). In this and in subsequent isotope plots the broken lines indicate solar isotopic ratios.

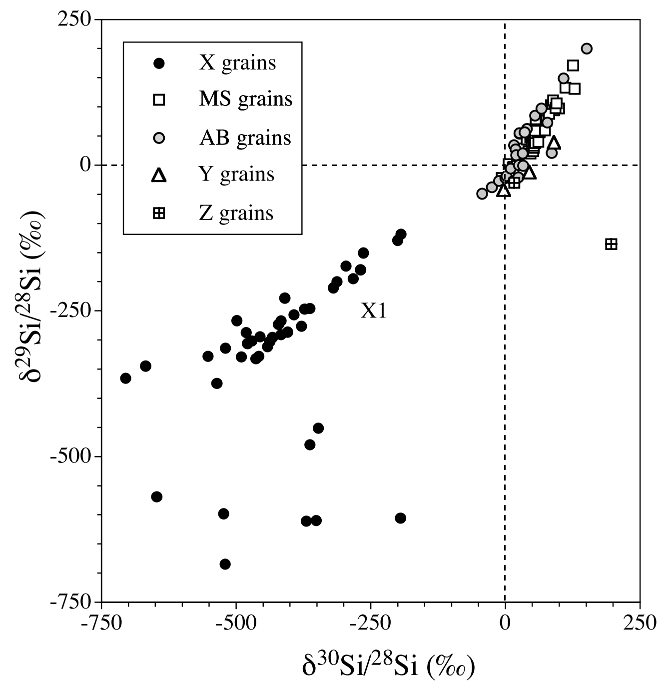

FIG. 3.—Si isotopic ratios of the grains analyzed in this study. Here and in subsequent isotopic ratio plots the ratios are plotted as so-called δ-values, deviations from the normal (solar) isotopic ratios in parts per thousand (permil, ‰). Most X grains plot close to a line of slope ~0.6, and are called X1 grains (Lin et al. 2002).

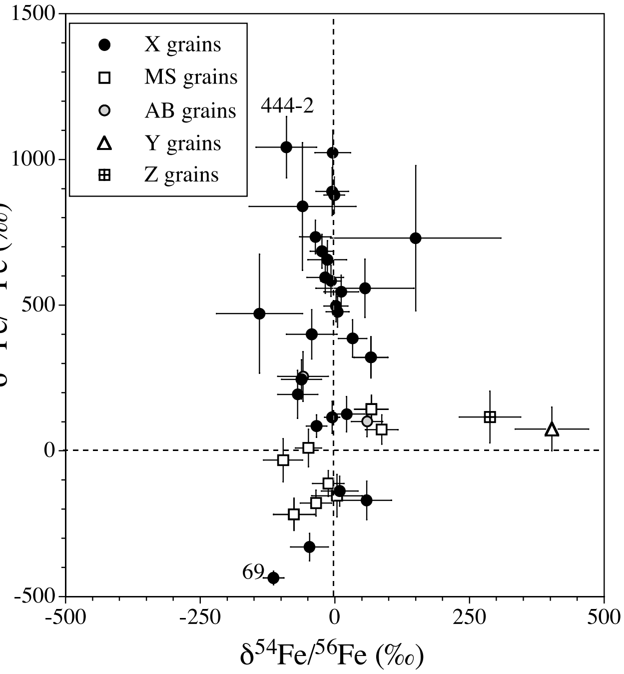

FIG. 4.—Three-isotope plot of Fe isotopic ratios of presolar SiC grains. In this figure and in Figs. 6, 16, 18, 19, and 20 we plot only grains whose isotopic ratios differ from normal ratios by more than 2 σ in one coordinate or the other. Here and in subsequent isotope plots error bars are 1 σ.

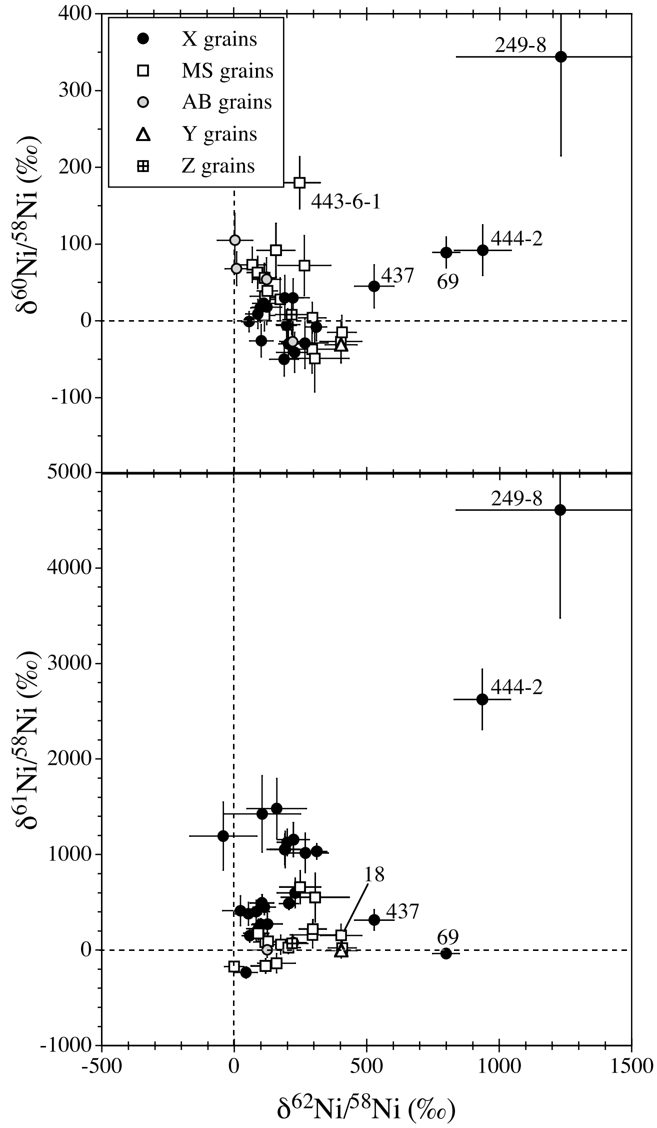

FIG. 5.—Three-isotope plots of Ni isotopic ratios measured in presolar SiC grains. A few unusual grains discussed in the text are labeled.

2004); however, the X grain showed marginal, small (40‰ and 32‰) enhancements in both ratios.

Ni isotopic ratios, again only of anomalous grains, are plotted in Figure 5. The largest anomalies, mostly excesses, are seen in ^{61}Ni. We found only excesses for ^{62}Ni. Except for four grains, ^{62}Ni excesses in X grains are not larger than those in other grain types. Grain 69 is peculiar in that it has a large ^{62}Ni excess and a clearly resolved ^{60}Ni excess, but a normal ^{61}Ni/^{58}Ni ratio. In addition, it also exhibits deficits in ^{54}Fe and ^{57}Fe (see Fig. 4). We will discuss it in more detail below. The four X grains with the largest ^{62}Ni excesses (249-8, 444-2, 69, 437) also have ^{60}Ni excesses, but the ^{60}Ni/^{58}Ni ratios of the other X grains are close to solar and smaller that those of a few AB and mainstream grains. However, this situation changes if we use larger-than-solar ^{58}Fe/^{56}Fe ratios for the ^{58}Fe correction on ^{58}Ni for the X grains, which shifts the Ni isotopic ratios to larger values. Mainstream grain 443-6-1 has large excesses in ^{60}Ni, ^{61}Ni, and ^{62}Ni, but normal Fe isotopic ratios. There are no well-defined correlations between the Ni isotopic ratios except that the two X grains with the largest ^{62}Ni excesses (249-8 and 444-2) also have the largest ^{60}Ni and ^{61}Ni excesses. On the other hand, X grains with normal ^{62}Ni/^{58}Ni ratios have large ^{61}Ni excesses and many X grains with ^{62}Ni excesses have normal ^{60}Ni/^{58}Ni ratios.

In Figures 6*a* and 6*b* we show correlation plots between the Ni and the Fe isotopic ratios. Because most X grains have ^{54}Fe/^{56}Fe ratios close to solar, there are no strong correlations between the Ni isotopic ratios and ^{54}Fe/^{56}Fe. We have already pointed to the peculiar isotopic composition of grain 69. The Y and Z grains, which have the largest ^{54}Fe excesses, have substantial ^{62}Ni excesses. We can see a correlation between ^{57}Fe/^{56}Fe and ^{61}Ni/^{58}Ni ratios in the sense that all the grains with ^{57}Fe excesses also have ^{61}Ni excesses. However, their ratios do not plot along a simple correlation line, and there is considerable scatter. There is scarcely any correlation between the ^{57}Fe/^{56}Fe and the ^{60}Ni/^{58}Ni and ^{62}Ni/^{58}Ni ratios, except for the two X grains (444-2 and 249-8) with large ^{57}Fe and ^{62}Ni excesses. Grain 249-8 also has a large ^{60}Ni excess.

We found that isotopic ratios, especially the ^{57}Fe/^{56}Fe ratio, depend on the elemental compositions of the grains. Figure 7*a* shows δ^{57}Fe/^{56}Fe values of X grains as a function of their Ni/Fe ratios. The Ni/Fe ratio is normalized to the solar ratio (Anders & Grevesse 1989). Two remarkable facts can be seen in the graph. First, the Ni/Fe ratios of the X grain are *much* higher than the solar ratio. Second, it is apparent that the grains with large ^{57}Fe excesses have smaller Ni/Fe ratios than grains with no or moderate ^{57}Fe excesses. Co/Fe ratios in the grains are also much higher than the solar ratio, but there is no obvious correlation between ^{57}Fe/^{56}Fe ratios and Co/Fe ratios (Fig. 7*b*). The situation becomes even more intriguing if one plots the Ni versus the Fe contents of the grains (Figs. 8*a* and 8*b*). Almost all mainstream and AB grains and many X grains plot along a single line. No grains plot above this line, but the remaining X grains plot to the right of it. With a few exceptions, these grains have large ^{57}Fe excesses. The numbers written next to these X grains in the two plots are their δ^{57}Fe/^{56}Fe values. The correlation line has a slope (Ni/Fe ratio) of $\sim$5.5, much higher than the solar Ni/Fe ratio of 0.059 (Anders & Grevesse 1989).

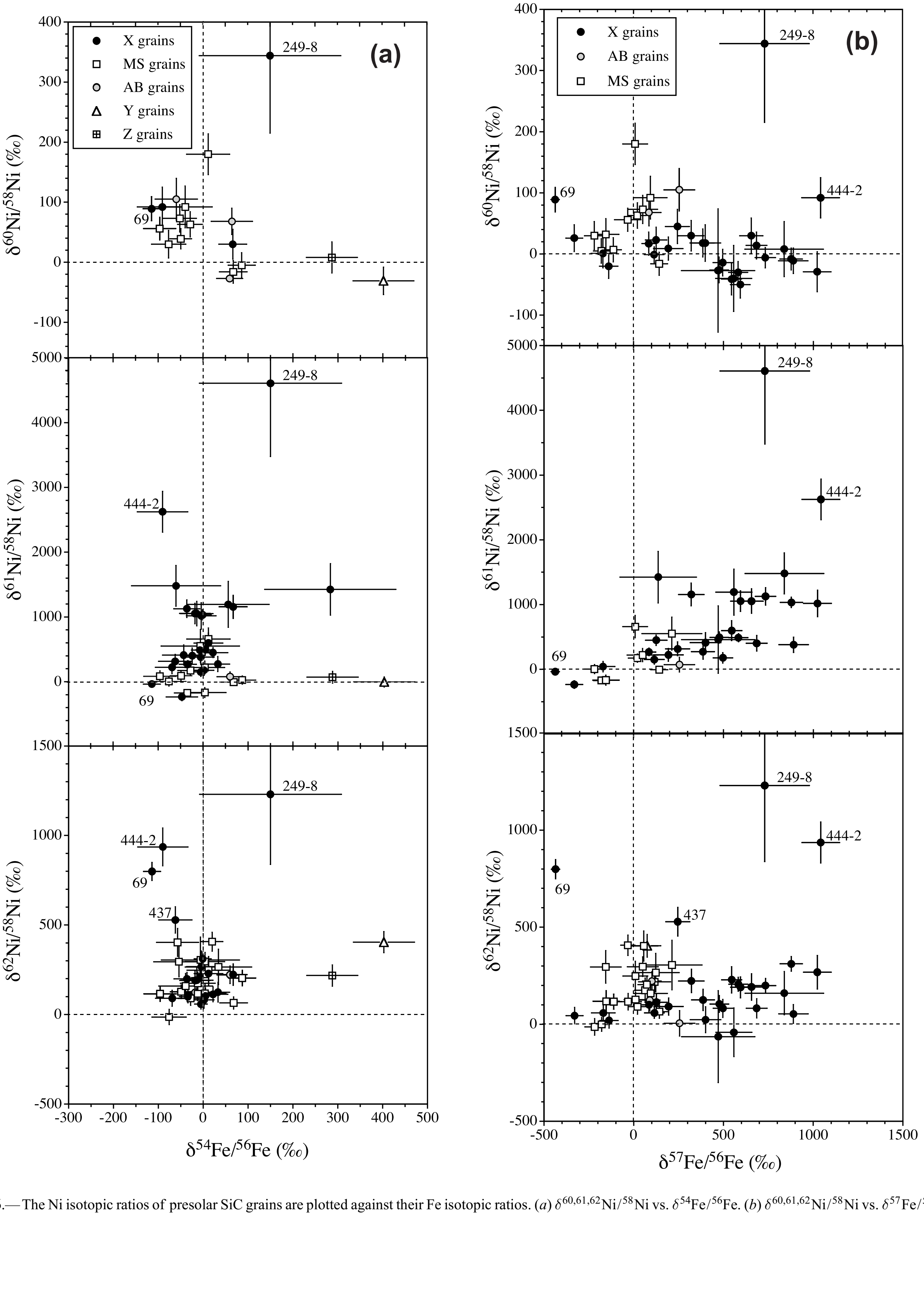

FIG. 6.—The Ni isotopic ratios of presolar SiC grains are plotted against their Fe isotopic ratios. (*a*) $\delta^{60,61,62}Ni/^{58}Ni$ vs. $\delta^{54}Fe/^{56}Fe$. (*b*) $\delta^{60,61,62}Ni/^{58}Ni$ vs. $\delta^{57}Fe/^{56}Fe$.

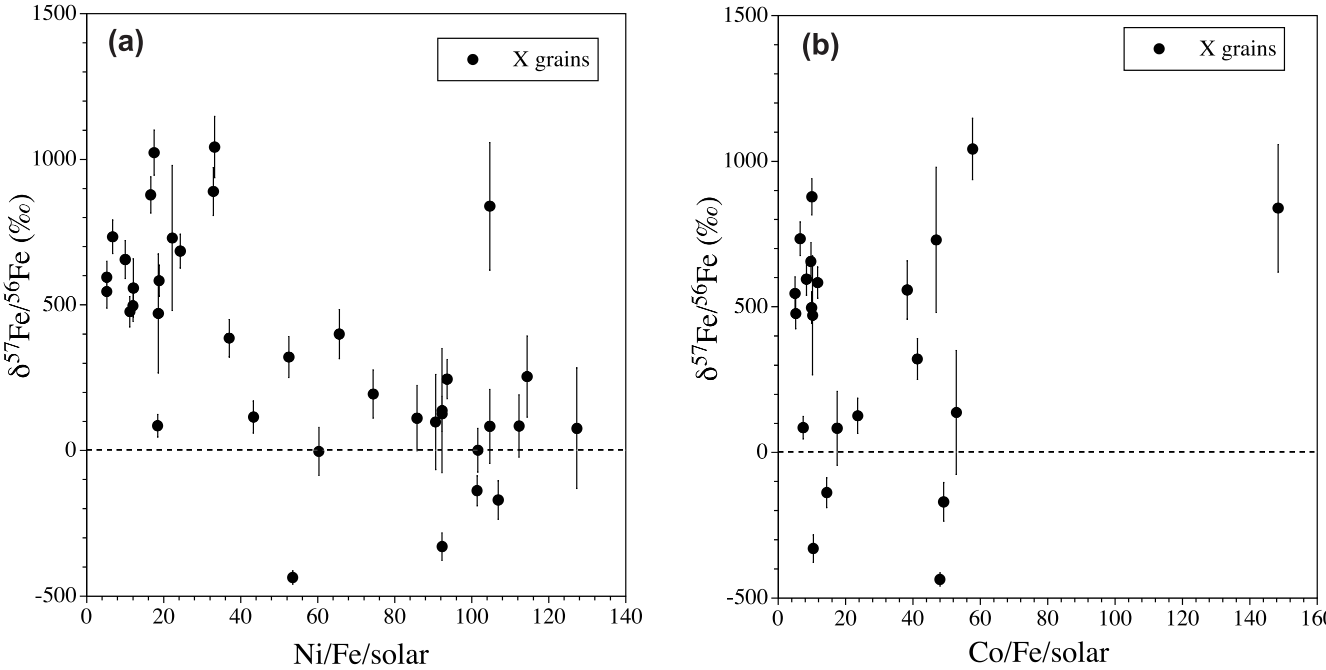

FIG. 7.—(*a*) $^{57}Fe/^{56}Fe$ ratios of X grains are plotted against their Ni/Fe ratio normalized to the solar ratio (Anders & Grevesse 1989). (*b*) $^{57}Fe/^{56}Fe$ ratios vs. normalized Co/Fe ratios. Both the Ni/Fe and Co/Fe ratios in the grains are much higher than the solar ratios.

An inspection of depth profiles of the ion signals during the NanoSIMS measurements shows that Fe excesses relative to the Ni versus Fe correlation line in Figure 8 are associated with Fe-rich subgrains or clusters of subgrains inside of the SiC grains. An example is shown in Figure 9*a*, where we plot the ion signals of ^{28}Si and some of the Fe isotopes of the X grain 97 as a function of measurement time. As the primary beam sputters through the SiC grain, an Fe-rich subgrain is exposed. However, the large increase of the Fe signal is not followed by a corresponding increase of the Ni signal. Outside of the Fe-rich subgrain the Ni/Fe ratio is ~5, close to the slope of the correlation line in Figure 8*a* and 8b. In other words, these portions of the grain would plot on the correlation line in Figure 8; the Fe excess in the subgrain shifts the total composition of the grain to the right of this line. The composition of the subgrain alone plots even more to the right (Fig. 8*a*). The whole grain 97 has an ^{57}Fe excess of 890‰.

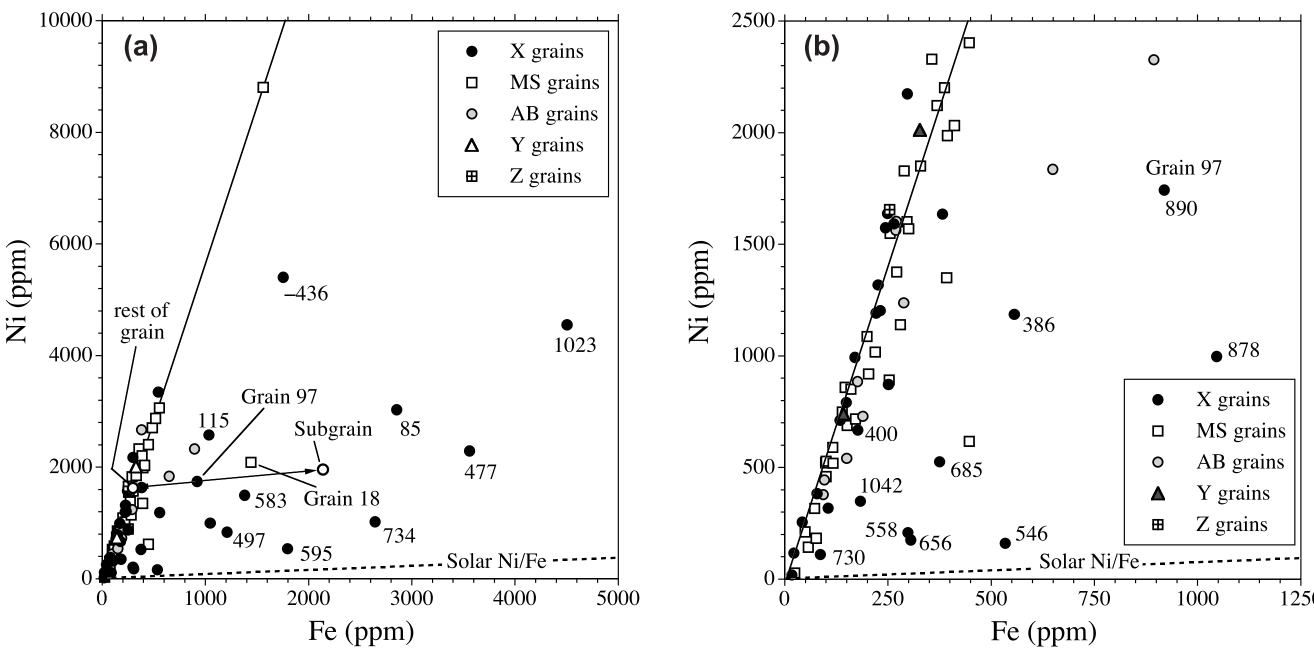

FIG. 8.—Plot of the Ni and Fe concentrations measured in presolar SiC grains. (*b*) shows a restricted region of the plot shown in (*a*). The solid line is a correlation line through the grains with the highest Ni/Fe ratios. Mostly X grains plot to the right of this line. Mainstream grain 18 is an exception. Also shown is the line with a solar Ni/Fe ratio. All grains plot above this line. The $\delta^{57}Fe/^{56}Fe$ values of many X grains are written next to the grain symbols. X grain 97 contains an Fe-rich subgrain (see Fig. 9). The filled symbol for this grain indicates the Ni-Fe composition of the whole grain, the open symbol that of the subgrain. The Ni-Fe composition of the SiC grain outside of the Fe-rich subgrain would plot close to the correlation line.

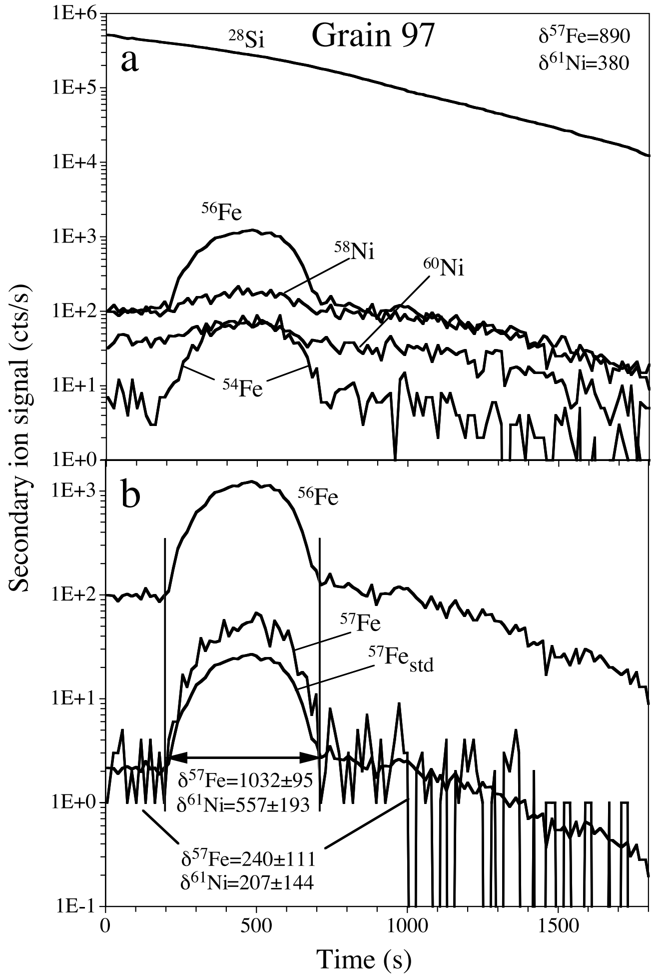

FIG. 9.— Depth profiles of Si, Fe, and Ni isotopes through X grain 97. The bottom panel shows measured Fe isotope signals. Also shown is a line obtained by multiplying the ^{56}Fe signal with the solar ^{57}Fe/^{56}Fe ratio (labeled "^{57}Fe$_{std}$"). It is apparent that in the region of the Fe-rich subgrain ^{57}Fe is enhanced. Both δ^{57}Fe/^{56}Fe and δ^{61}Ni/^{58}Ni values are much higher in the subgrain than outside.

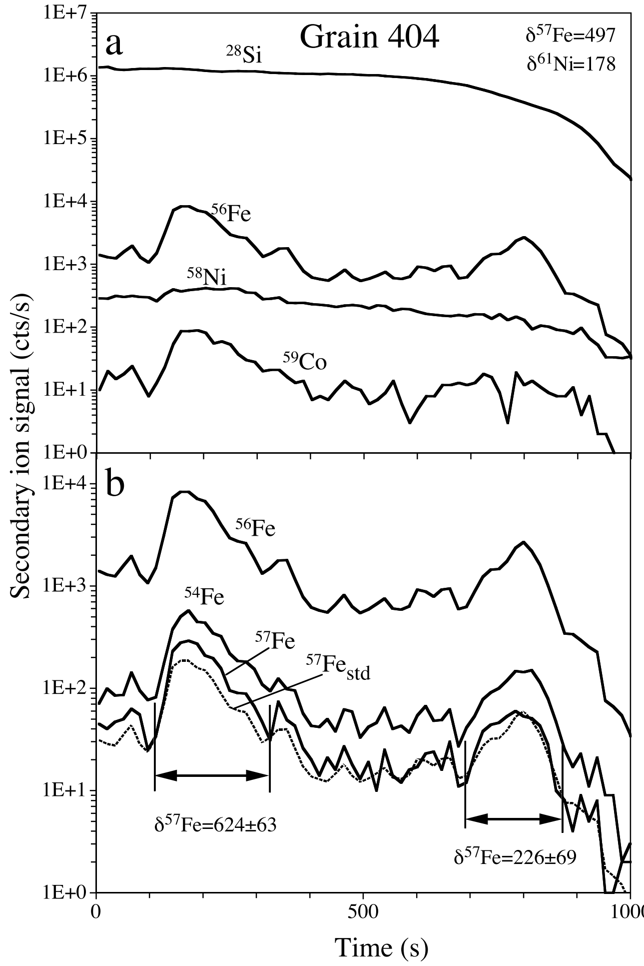

FIG. 10.— Depth profiles of Si, Fe, Co, and Ni isotopes through X grain 404. The grain contains two Fe-rich regions (the first is also rich in Co), which differ in their δ^{57}Fe/^{56}Fe values. The distribution of Ni in this SiC grain is very different from that of Fe and Co.

In Figure 9*b*, we plot the depth profiles of ^{56}Fe and ^{57}Fe. If we plot a line obtained by multiplying the ^{56}Fe signal with the solar ^{57}Fe/^{56}Fe ratio, it becomes apparent that the measured ^{57}Fe signal plots above this line in the region of the Fe-rich subgrain. If we calculate the ^{57}Fe/^{56}Fe ratio in the subgrain and in the region outside of the subgrain, we obtain δ^{57}Fe/^{56}Fe values of 1032‰ and 240‰, respectively. It is clear that in this grain the ^{57}Fe/^{56}Fe ratio is heterogeneously distributed and the ^{57}Fe excess is mostly carried by the Fe-rich subgrain.

Another example of internal Fe isotopic heterogeneity within a given X grain (grain 404) is shown in Figure 10, where two Fe-rich subgrains have different ^{57}Fe/^{56}Fe ratios. Similar to grain 97, the Ni in this grain is fairly uniformly distributed. Interestingly, in the first subgrain the increase in the Fe signal is accompanied by an increase in the Co signal. This is not clearly the case for the second Fe-rich subgrain. Thus, the Fe/Co ratio varies among different subgrains. In all X grains with Fe-rich subgrains, the Ni signal is completely uncorrelated with the Fe signal.

A grain that is different from the above two examples is X grain 82-1. Although the Fe and Ni signals in this grain are also not well correlated and Fe shows a large excess over Ni (Fig. 11*a*) relative to the correlation line in Figure 8*a*, the ^{57}Fe and ^{61}Ni excesses observed in this grain are fairly uniformly distributed throughout the grain (Figs. 11*b* and 11*c*). In contrast to the first subgrain in grain 404 (Fig. 10*a*), the profile of Co in grain 82-1 correlates better with Ni than with Fe (Fig. 11*a*).

Isotopic heterogeneity within a given SiC grain is not restricted to grains with ^{57}Fe excesses. An example of this observation is demonstrated by the depth profiles observed in X grain 69 (Fig. 12). This grain has already been mentioned above because it has ^{54}Fe and ^{57}Fe deficits, essentially normal ^{61}Ni/^{58}Ni, and a large ^{62}Ni excess. As can be seen in Figure 12*b*, the ^{57}Fe depletion is larger in the second Fe-rich region than in the first one. In contrast, the ^{62}Ni excess appears to be fairly uniformly distributed throughout this grain (Fig. 12*c*).

The X grain 85 has deficits in both ^{57}Fe and ^{61}Ni. This grain does not have any obvious subgrains and the Fe and Ni are smoothly distributed throughout the grain (Fig. 13) with a Ni/Fe ratio close to 5. In Figure 8*a* it plots on the Ni-Fe correlation line. The ^{57}Fe and ^{61}Ni depletions in this grain are uniformly distributed.

Most of the grains plotting to the right of the correlation line in Figure 8*a* are X grains. One exception is grain 18, a mainstream grain whose depth profiles are shown in Figure 14. There are two Fe-rich regions in this grain, of which the second one is quite pronounced, separated by a region with the canonical Ni/Fe ratio of 5. The increase of Fe in the second, but not the first, subgrain is accompanied by a smaller relative increase in Ni. In contrast, the Co signal shows the same relative increase as the Fe signal. It is noteworthy that this grain has an excess in ^{62}Ni but normal

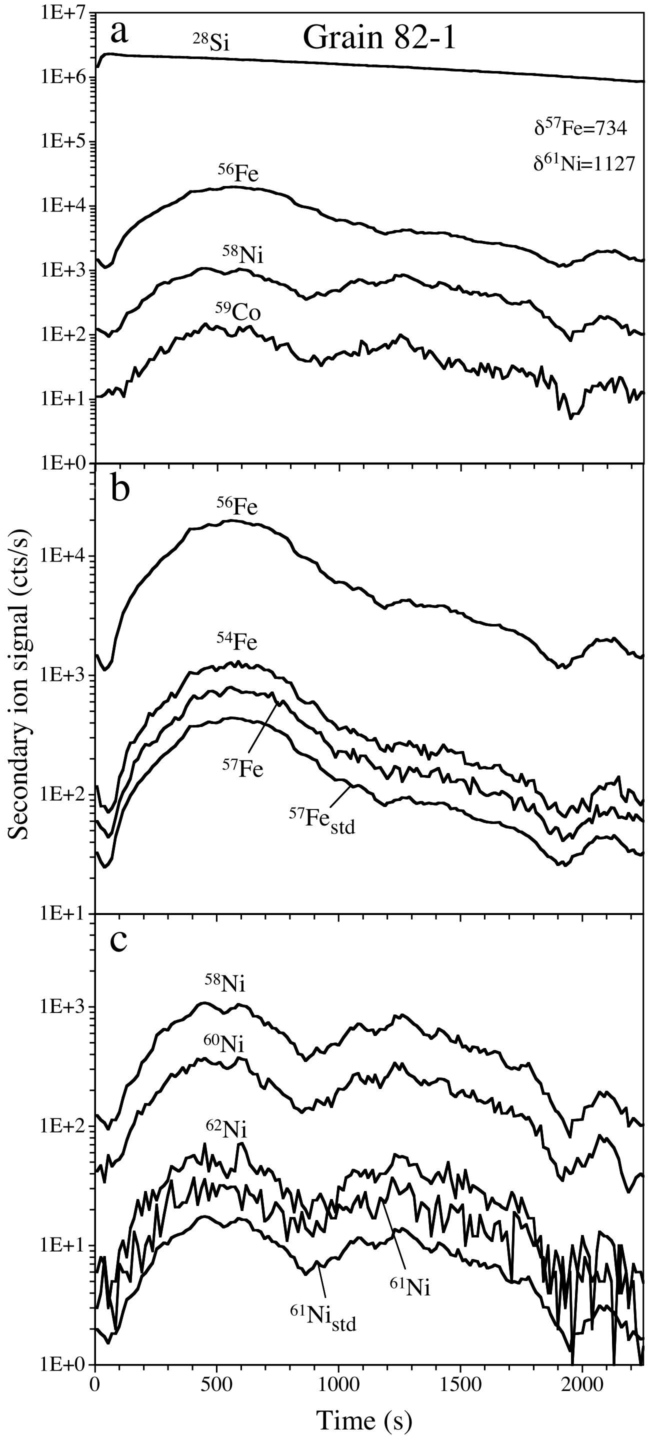

FIG. 11.— Depth profiles of Si, Fe, Co, and Ni isotopes through X grain 82-1. In this grain the distribution of Co is similar to that of Ni, and both elements differ from Fe. Grain 82-1 has excesses in (*b*) ^{57}Fe and (*c*) ^{61}Ni. The line labeled "^{61}Ni$_{std}$" is obtained by multiplying the ^{58}Ni signal with the solar ^{61}Ni/^{58}Ni ratio. Both the ^{57}Fe and ^{61}Ni excesses appear to be uniformly distributed throughout the SiC grain.

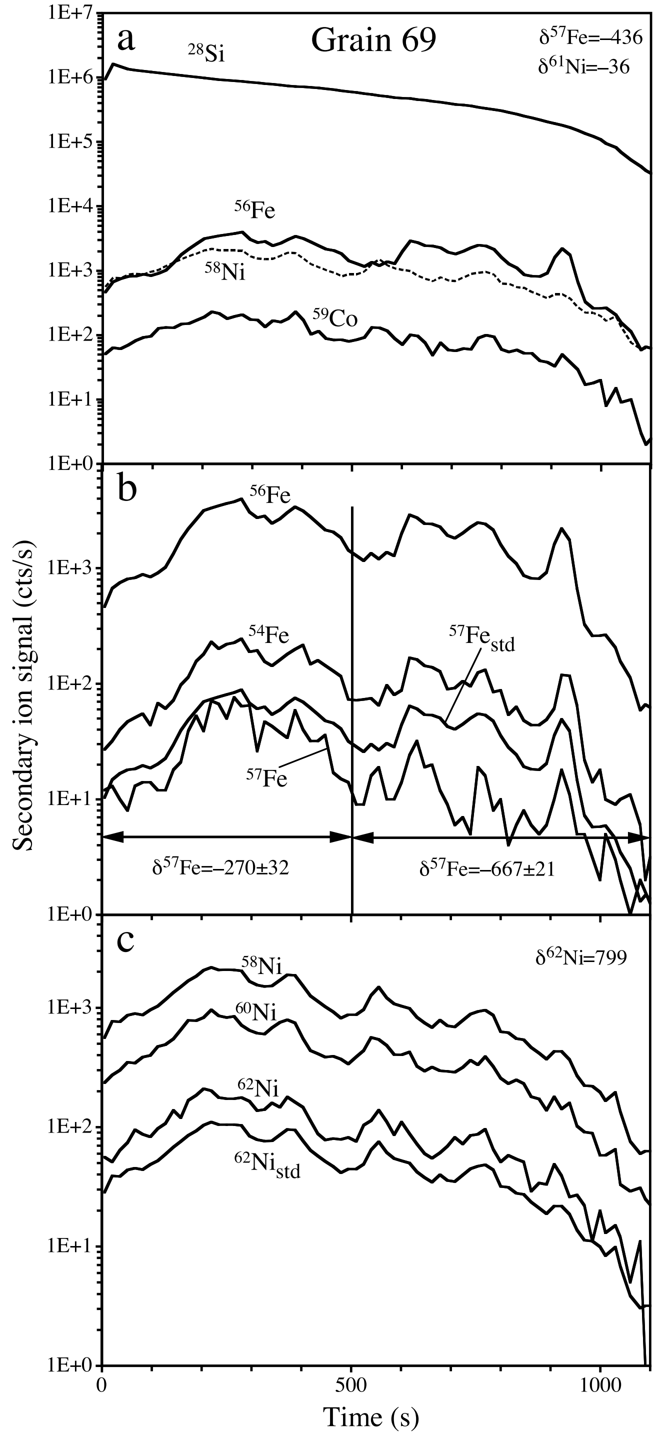

FIG. 12.— Depth profiles of Si, Fe, Co, and Ni isotopes through X grain 69. (*b*) This grain has a ^{57}Fe deficit, which is heterogeneously distributed. (*c*) It also has a ^{62}Ni excess, which seems to be uniformly distributed. The line labeled "^{62}Ni$_{std}$" is obtained by multiplying the ^{58}Ni signal with the solar ^{62}Ni/^{58}Ni ratio.

^{60}Ni/^{58}Ni and ^{61}Ni/^{58}Ni ratios (Fig. 5). Figure 14*b* shows that this excess is more or less uniformly distributed throughout the grain. Mainstream grain 443-6-1 has excesses in ^{60}Ni and ^{62}Ni (Fig. 5), but in contrast to grain 18, the Fe and Ni, fairly low in concentration (Table 2), are smoothly distributed throughout this grain.

In summary, there are large variations in the isotopic compositions of the grains, especially for the X grains, and the distributions of the isotopes within the grains. Two features in their Fe and Ni isotopic and elemental compositions distinguish X grains from the other grain types. First, Fe and Ni isotopic anomalies are much larger in X grains and second, many of the X grains have Fe-rich subgrains, and as a consequence lie to the right of the correlation line on which most of the other grains lie in a Ni versus

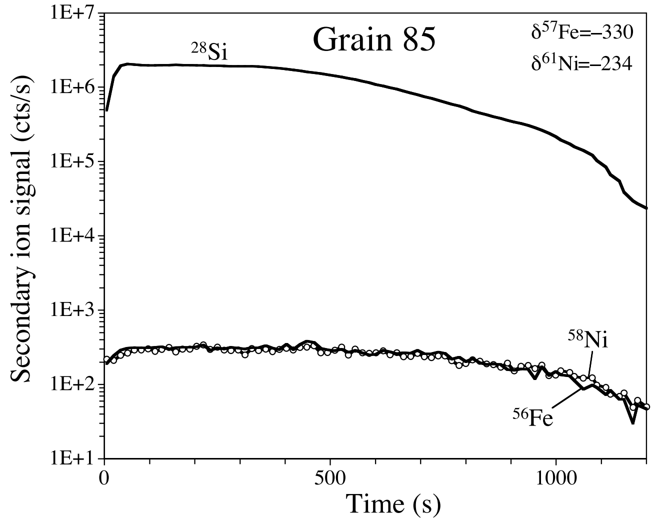

FIG. 13.—Depth profiles of Si, Fe, and Ni isotopes through X grain 85. In contrast to many other X grains, the distribution of Fe and Ni in this grain, which has deficits in ^{57}Fe and ^{61}Ni, is the same.

Fe concentration plot (Figs. 8*a* and 8*b*). These X grains typically contain the largest ^{57}Fe and ^{61}Ni excesses.

4. DISCUSSION

4.1. *Elemental Compositions*

We were surprised to find such high Ni concentrations in the grains, which in most cases exceed those of Fe. Previously, contents of Fe have been measured by SIMS in presolar SiC grains (Virag et al. 1992; Amari et al. 1995; Hoppe et al. 2000). Kashiv et al. (2001, 2002) and, more recently, Knight et al. (2008) determined concentrations of trace elements, including Fe and Ni, in presolar SiC grains by synchrotron X-ray fluorescence. Knight found that in most grains Ni concentrations exceed those of Fe (K. Knight 2008, private communication). Figures 8*a* and 8*b* show a line with the solar Ni/Fe ratio. The slope of the correlation line defined by most SiC grains exceeds the solar Ni/Fe ratio by a factor of ~90. The most likely stellar sources are Type II supernovae for X grains and AGB stars for mainstream grains. In the SN layers which contributed most material to the formation of X grains and in the envelope of C-rich AGB stars, the Ni/Fe ratio is believed to be close to solar. Thus, the Ni/Fe ratio of ~5.5 means that in most SiC Ni is fractionated over Fe by a factor of ~90 relative to the atmosphere in which the grains condensed.

The prevalent Ni/Fe ratio of ~5.5 in most mainstream and AB and many X grains must be the result of some chemical constraint. The mostly uniform distribution of Ni (and Fe in grains without Fe-rich subgrains or in regions without such subgrains) indicates that both elements are present as solid solutions (Lodders & Fegley 1995). Both Fe and Ni form carbides, Fe_3C and Ni_3C. Large fractionation between elements present in SiC relative to the source compositions has previously been observed. For example, Mg in presolar SiC grains is depleted by factors up to 1000 relative to Al and the solar abundances of these two elements (Amari et al. 1995). This has been explained by their very different chemical properties. Al is much more refractory than Mg and probably condenses into SiC as AlN (Lodders & Fegley 1995). However, Fe and Ni are much more similar in their physical and chemical properties, and if anything Ni is more volatile than Fe. It is thus completely unexpected that Ni shows such a large relative overabundance in most presolar SiC grains. At present we do not have a satisfactory explanation for this observation, but plan to investigate it in detail in a separate study.

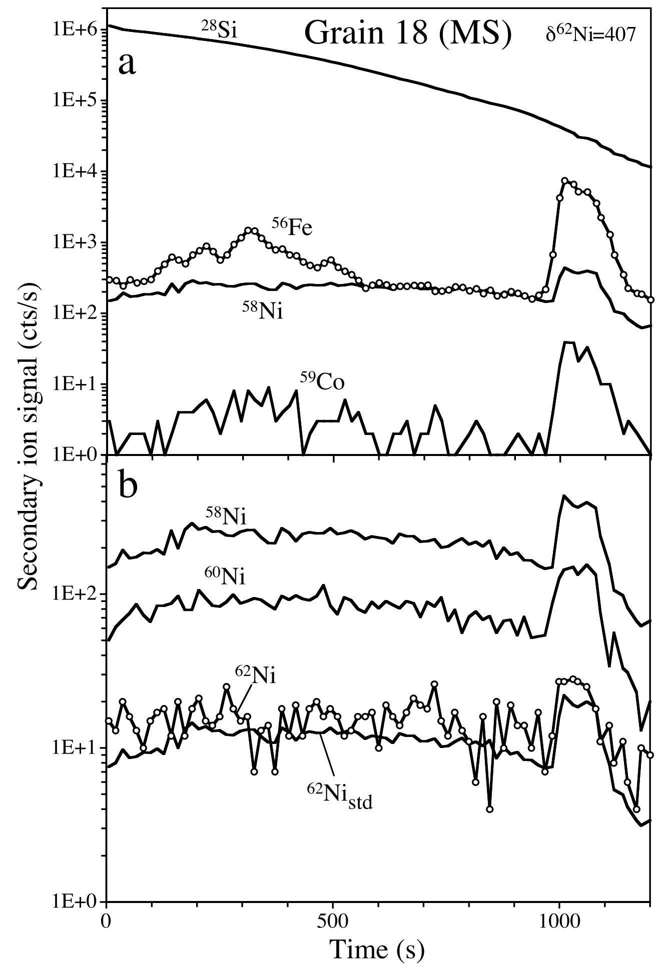

FIG. 14.—Depth profiles of Si, Fe, Co, and Ni isotopes through mainstream grain 18. While the first Fe-rich region does not show a corresponding increase in the Ni signal, the Fe-rich grain reached at ~1050 s is also rich in Co and Ni. There does not appear to be any spatial preference for the ^{62}Ni excess.

Fe-rich subgrains have previously been observed in transmission electron microscopy (TEM) studies within X grains (Hynes et al. 2006a). These subgrains show large variations in the Ni/Fe ratio, which range from 0.21 to 1.9. Because of the high general concentration of Ni throughout the grains, it is difficult to estimate the Ni/Fe ratio within the Fe-rich subgrains inferred from the depth profiles in the SiC grains of this study. There appears to be a slight Ni enhancement in the area of the Fe-rich subgrain in X grain 97 (Fig. 9*a*). Since equal $^{56}Fe^+$ and $^{58}Ni^+$ signals correspond to a Ni/Fe ratio of 5 (a consequence of the relative ion yields of Fe and Ni and the relative abundances of these two isotopes), the Ni/Fe ratio of the subgrain is estimated to be approximately 0.5. In a similar way, we can estimate that the Ni/Fe ratio in the first subgrain of X grain 404 (Fig. 10*a*) is about 0.12. In the region of the second subgrain, we cannot discern any corresponding excess in the $^{58}Ni^+$ signal. In X grain 82-1, we consider the subgrain corresponding to the bump in the $^{56}Fe^+$ signal between 2000 and 2200 s and obtain a Ni/Fe ratio of 0.66. In X grain 69 (Fig. 12*a*), some of the bumps in the $^{56}Fe^+$ signal are accompanied by bumps in the $^{58}Ni^+$ signal (e.g., at 380 and 760 s), with estimated Ni/Fe ratios of 2.3 and 2.0. For the subgrain at 920 s, we estimate a Ni/Fe ratio of 0.3. Finally in grain 18, a mainstream grain (Fig. 14*a*), the first Fe-rich region is not accompanied by any increase in the $^{58}Ni^+$ signal; however, the second Fe-rich subgrain contains Ni. For this subgrain, we obtain an estimated Ni/Fe ratio of 0.25. Similarly to Ni, Fe-rich subgrains also contain Co. For the first Fe-rich subgrain in grain 404 (Fig. 10*a*) we estimate a Co/Fe ratio of 0.024, for the last bump in grain 82-1 (Fig. 11*a*) we obtain Co/Fe = 0.031, and for the Fe-Ni-rich subgrain in grain 18 (Fig. 14*a*) we obtain a ratio of 0.025. Ti-rich subgrains have previously been observed during Ti isotopic measurements of mainstream grains (Gyngard et al. 2006). Apparently, mainstream grains contain also Fe-Ni-Corich subgrains. Although there are considerable uncertainties in our estimates of the Ni/Fe and Co/Fe ratios, it is obvious that the Ni/Fe ratio in subgrains covers a large range, confirming the TEM observations by Hynes et al. (2006a). The Co/Fe ratio seems to be more uniform, but we analyzed only a limited sample.

4.2. *Isotopic Compositions*

4.2.1. *Supernova Grains*

The X grains show large excesses in ^{57}Fe (Fig. 4) and ^{61,62}Ni, and smaller excesses in ^{60}Ni (Fig. 5). There are several zones in Type II supernovae that show these isotopic signatures. In Figure 15, we show the abundances of the Fe and Ni isotopes in the interior zones of a 25 $M_\odot$ supernova model by Rauscher et al. (2002). Different zones are labeled according to their most abundant elements (Meyer et al. 1995). It has previously been discussed (e.g., Zinner 1998, 2007; Yoshida & Hashimoto 2004) that contributions from different SN zones are required in order to explain the isotopic signatures of X grains. A contribution from the He/N zone is needed for the high ^{26}Al/^{27}Al ratios, a contribution from the He/C zone for the high ^{12}C/^{13}C and ^{15}N/^{14}N ratios, and a contribution from the Si/S zone (and possibly the Ni core) to explain the ^{28}Si excesses and the initial presence of ^{44}Ti in the grains.

4.2.1.1. Mixing with Material from the He/C Zone

Because Fe and Ni are relatively heavy, their isotopic abundances are not affected by core H burning during the hydrostatic phase and shell H burning in the He/N zone. As a consequence, the isotopic ratios of these elements in the H envelope and the He/N zone are still their original ratios, assumed to be solar (Fig. 15). As we enter the He/C zone from the He/N zone, the abundances of ^{57,58}Fe and ^{61,62}Ni increase abruptly. They increase further as we cross the He/C zone toward the O/C zone (Fig. 15). In contrast, the abundances of ^{54,56}Fe and ^{58,60}Ni decrease slightly at the border between the He/N and He/C zones and more rapidly close to the O/C zone. The reason for this behavior is slow capture of neutrons produced by the $^{13}C(\alpha,n)^{16}O$ and $^{22}Ne(\alpha,n)^{25}Mg$ reactions. It is well known that massive stars are the sources of the so-called weak component of the *s*-process (see The et al. [2007] and references cited therein). While the weak *s*-component mostly produces nuclei with atomic masses from 65 to 90, this process also strongly affects the Fe and Ni isotopes. Neutron capture in massive stars takes place during He core burning, as well as during convective shell C burning (The et al. 2000, 2007; Pignatari et al. 2006; Heil et al. 2008). As a consequence, the Fe and Ni isotopes in the He/C zone and the underlying O/C and O/Ne layers (Fig. 15) show strong signatures of the *s*-process. The ^{57,58}Fe and ^{60,61,62}Ni abundances increase whereas ^{56}Fe and ^{58}Ni abundances decrease. ^{54}Fe is bypassed by the *s*-process path and thus behaves like a *p*-only nuclide. Its original abundance decreases due to neutron capture.

One can explain the Fe and Ni isotopic ratios of X grains quite well by mixing material from the He/N and He/C zones. In Figures 16*a* and 16*b*, we plot, in addition to the grains' isotopic ratios, lines obtained by mixing material from the He/N zone with variable amounts from two layers of the He/C zone. Mix He/C-a uses a composition just below the He/N zone at interior mass 8.05 $M_\odot$ (see Fig. 15); mix He/C-b uses a composition close to the O/C zone, at interior mass 7.14 $M_\odot$. As can be seen, the ratios obtained from this mixing model cover those of most X grains quite well, considering that He/C layers between the two chosen layers will results in intermediate slopes of the mixing lines in Figure 16*b*. We have to keep in mind that Ni/Fe ratios vary within individual grains, as well as among different grains. Thus, we have to allow for fractionation between Ni and Fe in the mixing models in order to cover the whole range of most of the data points in Fig. 16*c*.

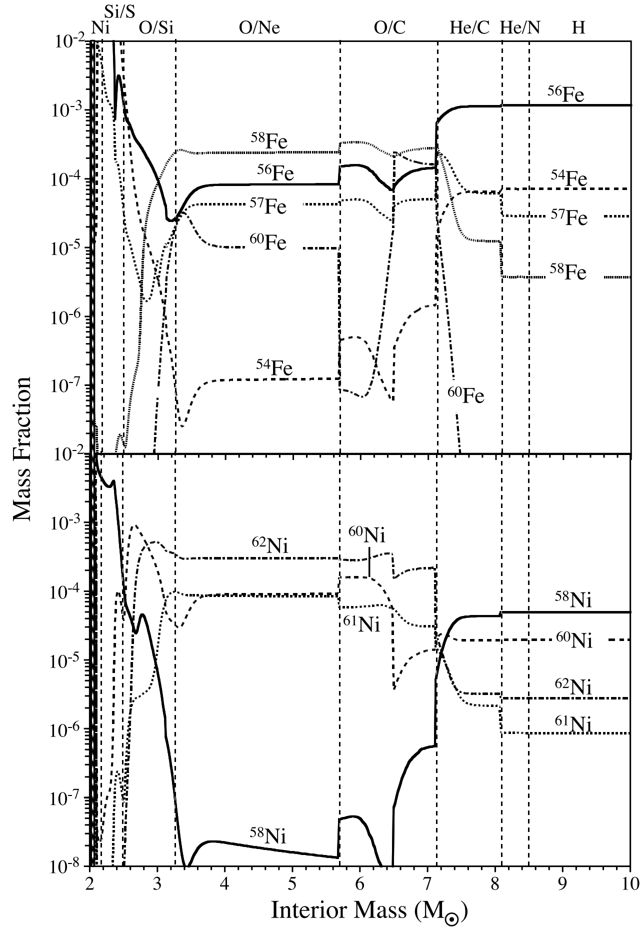

FIG. 15.—Distributions of Fe and Ni isotopes in different interior zones of the 25 $M_\odot$ SN model by Rauscher et al. (2002). The vertical coordinate is the mass fraction of a particular isotope, the horizontal coordinate the interior mass in solar mass units. The different zones are labeled according to the two most abundant elements (Meyer et al. 1995).

The X grains with ^{57}Fe deficits are exceptions to this mixing model, especially grain 69. The Ni isotopic ratios of the latter can be explained by admixture of material from the O/C zone, but not the Fe isotopic ratios. As can be seen in Figure 15, the abundance of ^{62}Ni becomes very high in this zone. In addition, the outer layer of the O/C zone is rich in ^{60}Fe, a radionuclide with a half-life of 1.5 Myr, which, if it would have been incorporated into grains, decays into ^{60}Ni. In Figures 16*a*–16*c*, we plot lines resulting from mixing material from the He/N zone with material from the O/C zone at interior mass 7.0 $M_\odot$. In the top panel of Figure 16*b*, we include the contribution from ^{60}Fe. This contribution depends on the Ni/Fe ratios; we plot lines for the extreme ratios 0.3 and 7.3 found in X grains (Table 2). The range in the

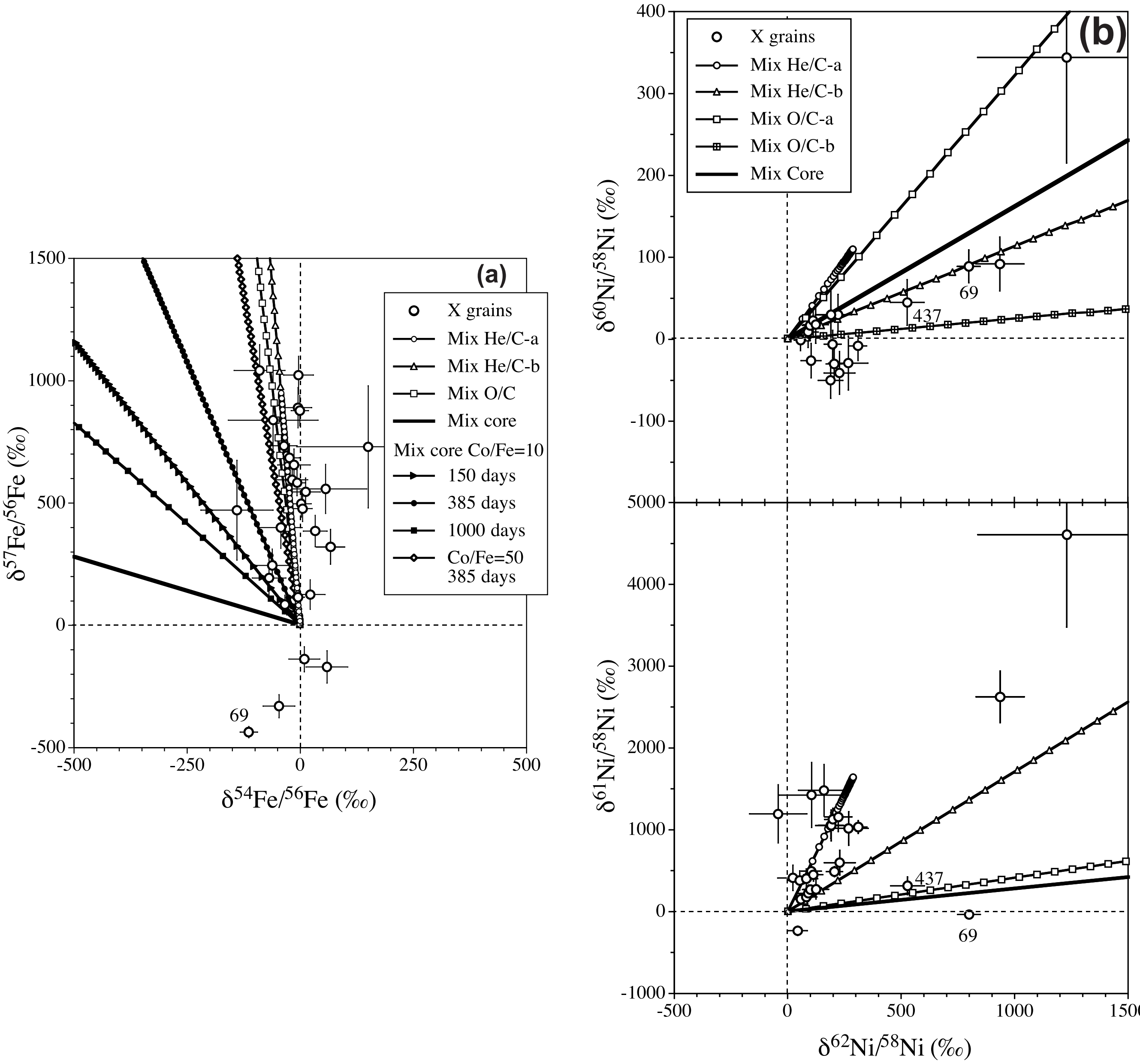

FIG. 16.—Fe and Ni isotopic ratios of X grains are compared with predictions from mixing models for the 25 $M_\odot$ SN by Rauscher et al. (2002). The labels "Mix a" and "Mix b" signify mixtures of material from the He/N zone with varying fractions from two different layers of the He/C zone. "Mix O/C" indicates a mix between the He/N and O/C zones. In (*b*) "Mix O/C-a" and "Mix O/C-b" correspond to mixtures for the two extreme values of the Ni/Fe ratios found in X grains. "Mix core" stands for a mixture of He/N matter with varying fractions of material from the Ni core. The lines labeled "150 days," "385 days," and "1000 days" are also for He/N-Ni core mixtures, but assume elemental fractionation of a factor of 10 between Co and Fe, and are for different condensation times of Co and Fe into the grains after the SN explosion. The line labeled "Co/Fe = 50, 385 days" expresses the isotopic ratios for He/N-Ni core mixtures with an assumed Co/Fe fractionation factor of 50 and a condensation time of 385 days after the explosion.

δ^{60}Ni/^{58}Ni versus δ^{62}Ni/^{58}Ni plot covered by the O/C-He/N mix is similar to that covered by the He/C-He/N mix. The situation is quite different for the δ^{61}Ni/^{58}Ni versus δ^{62}Ni/^{58}Ni plot (Fig. 16*b*, *bottom*) where only grains 437 and 69 plot close to the O/C-He/N mixing line. A contribution of only 0.65% from the O/C layer would result in δ^{62}Ni/^{58}Ni = 525‰, δ^{61}Ni/^{58}Ni = 213‰, δ^{60}Ni/^{58}Ni = 12‰ if we assume the Ni/Fe ratio of 5.4 measured in grain 437. For Ni/Fe = 3.1, measured in grain 69, and a 1% contribution from the O/C layer, we obtain δ^{62}Ni/^{58}Ni = 785‰, δ^{61}Ni/^{58}Ni = 326‰, δ^{60}Ni/^{58}Ni = 30‰.

However, mixing with material from the O/C zone does not reproduce the Fe isotopic compositions of these two grains and of X grains in general. The mixing line in Figure 16*a* is close to the He/N-He/C mixing line, but the δ^{57}Fe/^{56}Fe value reached when δ^{62}Ni/^{58}Ni reaches 1500‰ is only 35‰. A mix with a δ^{57}Fe/^{56}Fe value of 1000‰, reached by some X grains, would have a corresponding δ^{62}Ni/^{58}Ni value of 50,000‰, far above any values observed in the grains. The O/C-He/N mixing line in Figure 16*c* misses essentially all the X grains and, for δ^{62}Ni/^{58}Ni less than 1500‰, ranges only up to δ^{61}Ni/^{58}Ni = 620‰. Furthermore, O/C-He/N mixing cannot explain the ^{57}Fe deficit observed in grain 69 (Figs. 16*a* and 16*c*). The ^{57}Fe deficits in X grains present a general problem and we shall return to this topic below.

Evidence for the initial presence of several short-lived radionuclides has been found in presolar grains (e.g., Zinner et al. 2006a), but we cannot add ^{60}Fe to the list. SiC X grains are not

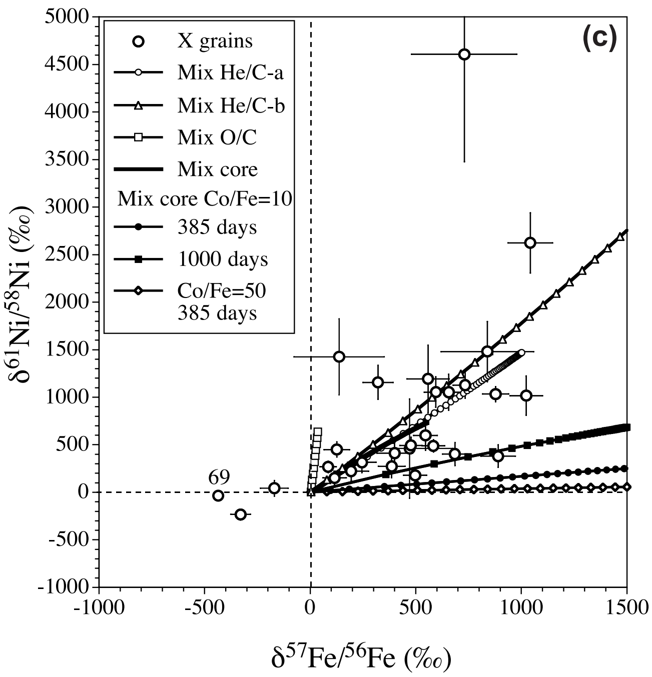

FIG. 16—*Continued*

good samples for a search for ^{60}Fe. The Fe/Ni ratios in these grains are much too low for any ^{60}Ni excesses originating from ^{60}Fe decay to be observable. The X grains 437 and 69 *could* carry some radiogenic ^{60}Ni, but we cannot establish any incontrovertible evidence for it. As discussed above, the Fe isotopic ratios of these two grains do not support mixing with material from the O/C zone. The upper O/C mixing line in Figure 16*a* is for a Fe/N ratio of 3.3. If this ratio were 100, the line would be much steeper and ^{60}Ni excesses might be much larger than the anomalies in any other Ni isotopes. This would be analogous to the situation for the Al-Mg system in presolar SiC and corundum grains. In such grains, the Al/Mg ratio can reach values in excess of 1000, and in some grains, Mg consists mostly of ^{26}Mg from the decay of ^{26}Al.

In summary, admixture of the O/C cannot explain the Fe and Ni isotopic ratios of the X grains we analyzed and we cannot claim any evidence for the prior presence of ^{60}Fe. An additional problem to be discussed below is that the O/C zone is extremely rich in ^{58}Fe, and the correction for ^{58}Fe to the ^{58}Ni signal would become enormous. The Fe and Ni isotopic compositions of the O/Ne and O/Si zones also do not fit the isotopic ratios measured in the X grains; ^{62}Ni is too abundant and ^{57}Fe not abundant enough. In addition, contributions from these zones would result in O/C ratios being larger than unity and SiC grains would not condense under such conditions.

4.2.1.2. Mixing with Material from the Core

Let us next look at the innermost zones of the supernova, where nuclear reactions approach a quasi-statistical equilibrium (QSE) and full nuclear statistical equilibrium (NSE), producing the Fe-peak elements (see, e.g., Meyer & Zinner [2006]; for a discussion of the nucleosynthesis of the Fe isotopes in these zones, see Clayton et al. 2002). In this regime, the abundances of the different isotopes are mostly determined by their binding energies. In Figure 17, we plot the abundances of the Fe and Ni isotopes in the inner zones of the Rauscher et al. (2002) 25 $M_{\odot}$ supernova model. We plot the so-called total abundances after the decay of unstable precursors. At the time of the SN explosion, the core

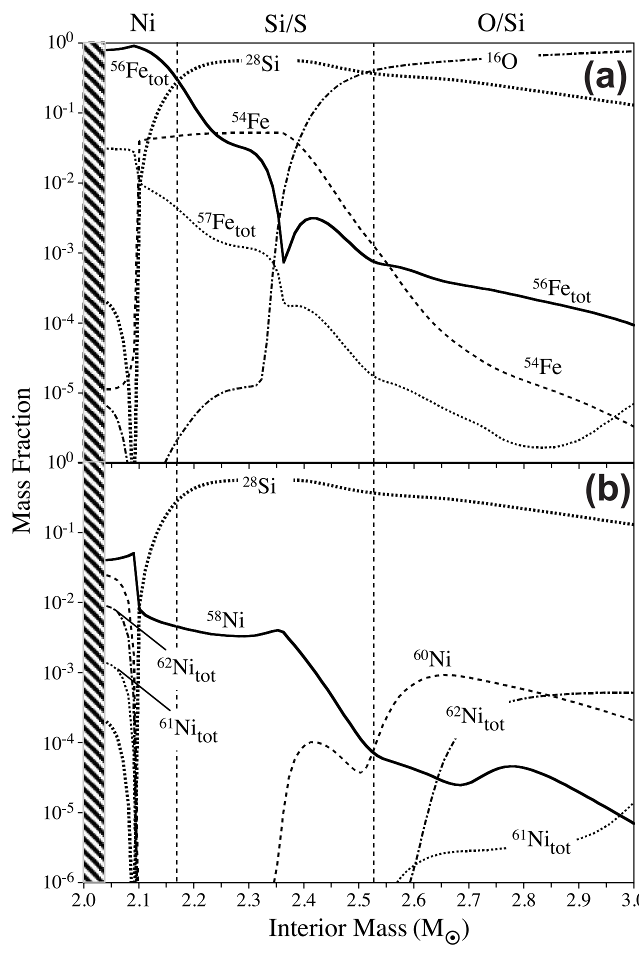

FIG. 17.—Distributions of O, Si, Fe, and Ni isotopes in the innermost zones of the 25 $M_{\odot}$ SN model by Rauscher et al. (2002). For $^{56,57}Fe$ and $^{61,62}Ni$ we plot the total fractions after the decay of radioactive precursors. The hatched region below ~2.035 $M_{\odot}$ SN lies below the so-called mass cut. Only material above the mass cut is believed to be ejected.

consists mostly of ^{56}Ni, which with a half-life of 5.9 days decays into ^{56}Co. ^{56}Co in turn with a half-life of 77.3 days decays into ^{56}Fe. In a similar way, ^{57}Fe in the core derives from the decay of ^{57}Ni ($T_{1/2} = 35.6$ hr) and its decay product ^{57}Co ($T_{1/2} = 272$ days). Based on the correlation between ^{49}Ti excesses in X grains and their V/Ti ratios, Hoppe & Besmehn (2002) have argued that some ^{49}Ti excesses originate from the decay of short-lived ^{49}V ($T_{1/2} = 330$ days). These grains therefore must have formed within a few months after the SN explosion. Since the half-life of ^{57}Co is similar to that of ^{49}V, ^{57}Fe could have been incorporated into the grains as ^{57}Co if they received significant contributions from the SN core. ^{61}Ni and ^{62}Ni also receive contributions from radioactive precursors, which, however, decay on a timescale of hours.

Since the core is so rich in Fe and Ni, even an admixture of 1% of core material to material from the He/N zone will change the Fe and Ni isotopic compositions significantly. The isotopic composition of the inner core (Fig. 17) shows excesses of ^{57}Fe and ^{60,61,62}Ni relative to solar, corresponding to δ^{57}Fe/^{56}Fe = 560‰, δ^{60}Ni/^{58}Ni = 430‰, δ^{61}Ni/^{58}Ni = 740‰, and δ^{62}Ni/^{58}Ni = 2640‰. Unfractionated admixture of core material cannot reproduce the Fe isotopic ratios of the X grains. The main problem is that the ^{54}Fe abundance in the inner core is very low, and any mix would have large ^{54}Fe deficits not shown by the grains. Figures 16*a* and 16*b* show mixing lines obtained by mixing material from the inner core with material from the He/N zone. The mixing line in Figure 16*a* misses all X grains and that in Figure 16*b* most X grains. The mix might be able to explain the ^{61}Ni/^{62}Ni ratios of grains 69 and 437 but not their ^{57}Fe/^{56}Fe ratios, and certainly not their ^{54}Fe/^{56}Fe ratios. In Figure 16*c*, the core mixing line is close to the first He/N-He/C mixing line, but the maximum predicted δ^{57}Fe/^{56}Fe and δ^{61}Ni/^{58}Ni values are too small to cover the range spanned by the grain data.

However, we note that the Co/Fe ratios, not only in X grains (Fig. 7*b*) but also in mainstream and AB grains, are much higher than the solar ratio (see Table 2). Thus, if X grains condensed at a time when ^{57}Co was still present while most of ^{56}Co had decayed into ^{56}Fe, and if Co is preferentially included into the grains, final ^{57}Fe excesses could be produced that are not accompanied by large ^{54}Fe deficits. In Figures 16*a* and 16*c*, we show also mixing curves obtained by mixing core material with material from the He/N zone under the assumption that Co and Ni condense into SiC 10 times more readily than Fe. The three lines correspond to formation times of 150, 385, and 1000 days after the explosion. After 150 days, there is still enough ^{56}Co present so that its inclusion in the grains, combined with the lack of ^{54}Fe from the core, results in substantial ^{54}Fe deficits accompanying ^{57}Fe excesses. A condensation time of 385 days after the explosion gives the maximum (negative) slope in Figure 16*a*. At this time, most of the ^{56}Co has decayed into ^{56}Fe, while there is still enough ^{57}Co present to result in ^{57}Fe excesses with minimal ^{54}Fe deficits. Even this line misses most X grain data. Finally, after 1000 days, a substantial amount of ^{57}Co has decayed into ^{57}Fe and the effect of Co/Fe fractionation is reduced. As the time of condensation increases, the mixing curves approach the line without any Co/Fe fractionation. Increasing the Co/Fe fractionation factor gives steeper mixing lines. Shown in Figure 16*a* is a mixing line with an assumed Co and Ni fractionation factor of 50 relative to Fe and the optimal condensation time of 385 days. This line comes close to the He/N-He/C mixing lines and the data points. However, as seen in Figure 7*b*, only a few X grains show such a large enrichment of Co over Fe compared to solar. This figure also shows that there is no correlation between ^{57}Fe excesses and Co/Fe ratios.

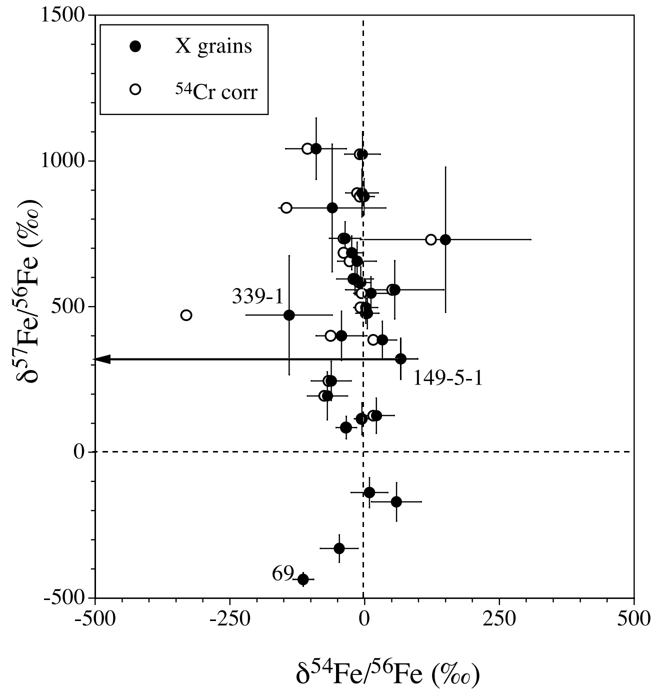

FIG. 18.—Fe isotopic ratios of X grains are plotted twice, once after correction for ^{54}Cr interference with ^{54}Fe under the assumption of a solar ^{54}Cr/^{52}Cr ratio (*filled circles*), the second time under the assumption that the ^{54}Cr/^{52}Cr ratio scales with the ^{57}Fe/^{56}Fe measured in the grains according to theoretical predictions for the He/C zone (*open circles*). Only in the two labeled grains are the changes larger than the 1 σ measurement errors.

The Ni isotopic ratios of the grains do not support mixing with core material. Because the radioactive precursors of ^{61}Ni and ^{62}Ni have short half-lives, they will have decayed by the time of grain formation. The Ni isotopes will therefore condense into the SiC grains as Ni. As a consequence, the Ni isotopic ratios predicted by core mixing are independent of Co/Fe and Ni/Fe fractionation, and the "Mix core" line shown in Figure 16*b* will remain the same, missing most of the grains. In Figure 16*c* elemental fractionation changes the core mixing curve because it affects the ^{57}Fe/^{56}Fe ratio. All mixing curves have small slopes, essentially missing the grain data. The reason is that elemental fractionation increases the ^{57}Fe/^{56}Fe ratio, while the ^{61}Ni/^{58}Ni remains the same with a maximum δ^{61}Ni/^{58}Ni of 740‰ of the core.

In summary, the Fe and Ni isotopic ratios observed in X grains cannot be satisfactorily explained by contributions from the inner core. Admixture from the He/C zone as discussed above is a more likely explanation for the observed isotopic compositions.

4.2.1.3. Effect of Interference Correction

As mentioned in § 2, we assumed solar ^{54}Cr/^{52}Cr and ^{58}Fe/^{56}Fe ratios in order to make corrections for the contributions of ^{54}Cr to ^{54}Fe and of ^{58}Fe to ^{58}Ni. If indeed admixture from the He/C zone is responsible for the ^{57}Fe and ^{61,62}Ni excesses observed in many grains, we can refine the corrections for the ^{54}Cr and ^{58}Fe interferences. Both of these isotopes are predicted to be enhanced in the He/C zone (for ^{58}Fe see Fig. 15). In order to obtain improved ^{54}Cr/^{52}Cr and ^{58}Fe/^{56}Fe ratios for the corrections, we scaled these ratios to the average ^{57}Fe/^{56}Fe ratio over the entire He/C zone in the 25 $M_{\odot}$ SN model by Rauscher et al. (2002), and multiplied them with the ^{57}Fe/^{56}Fe ratios measured in X grains with ^{57}Fe excesses.

Since ^{54}Cr/^{52}Cr ratios for individual grains obtained by this correction procedure are larger that the solar ratio, ^{54}Fe/^{56}Fe ratios corrected with these ratios will be smaller than the ratios we obtained with the solar ^{54}Cr/^{52}Cr ratio. Figure 18 shows the Fe

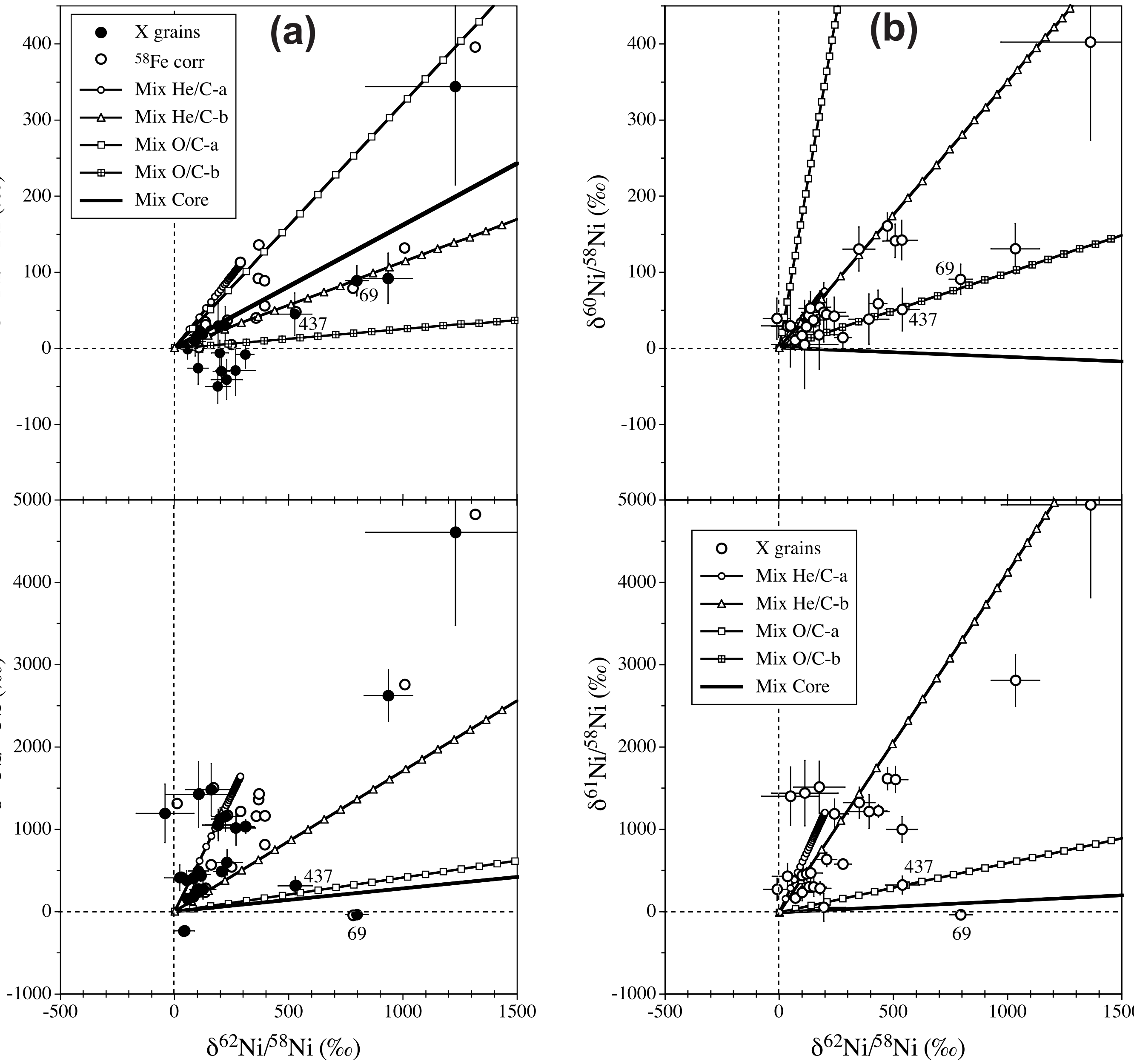

Fig. 19.—(*a*) Ni isotopic ratios of X grains are plotted twice, once after correction for ^{58}Fe interference with ^{58}Ni under the assumption of a solar ^{58}Fe/^{56}Fe ratio (*filled circles*), the second time under the assumption that the ^{58}Fe/^{56}Fe ratio scales with the ^{57}Fe/^{56}Fe measured in the grains according to theoretical predictions for the He/C zone (*open circles*). The lines predicted for various zone mixing shown in Fig. 16*b* are also shown here. (*b*) Ni isotopic ratios of X grains are compared with the results of mixing lines obtained for the 15 $M_\odot$ SN model by Rauscher et al. (2002). (*c*) X grain data and theoretical mixing lines for the 25 $M_\odot$ SN model and new neutron-capture cross sections for ^{60}Ni and ^{62}Ni (Corvi et al. 2002; Alpizar-Vicente et al. 2008).

isotopic ratios of X grains with ^{57}Fe excesses corrected in this way. The magnitude of the changes in the ^{54}Fe/^{56}Fe ratios vary from grain to grain because they depend on the ^{57}Fe/^{56}Fe ratio and the Cr/Fe ratio for a given grain. As can be seen, changes in ^{54}Fe/^{56}Fe ratios are minor in almost all cases, smaller than the 1 σ errors for the individual measurements. An exception is grain 149-5-1, which has a large Cr-rich subgrain where most of the signal at mass 54 originates from ^{54}Cr (Fig. 1). For this grain, correction with an increased ^{54}Cr/^{52}Cr ratio would result in a negative value for ^{54}Fe. The fact that the ^{54}Fe/^{56}Fe ratio in this grain obtained with a solar ^{54}Cr/^{52}Cr ratio is close to normal (Fig. 18) indicates that the subgrain has a solar ^{54}Cr/^{52}Cr ratio. It may have been a piece of contamination that was covered by the X grain and exposed as the primary O beam sputtered away the SiC grain.

Because ^{58}Ni is used as the reference isotope for our Ni isotopic ratios, a larger correction for ^{58}Fe results in a smaller ^{58}Ni value and an increase in δ^{i}Ni/^{58}Ni values. Figure 19 shows the Ni isotopic ratios of X grains obtained in this way, together with the ratios obtained under the assumption of solar ^{58}Fe/^{56}Fe ratios. As for the ^{54}Fe/^{56}Fe ratios, the changes in the Ni isotopic ratios differ among grains because they depend on the ^{57}Fe/^{56}Fe ratios and the Ni/Fe ratios of individual grains. As can be seen in Figure 19*a*, the new Ni isotopic ratios improve the agreement with theoretical expectations in that many negative δ^{60}Ni/^{58}Ni values have become positive values.

The abundances of ^{54}Cr and ^{58}Fe in the O/C and O/Ne zones are much higher than those in the He/C zone (e.g., Rauscher et al. 2002; for ^{58}Fe see also Fig. 15). On the other hand, the abundances of the reference isotopes ^{52}Cr and ^{56}Fe are much lower. A

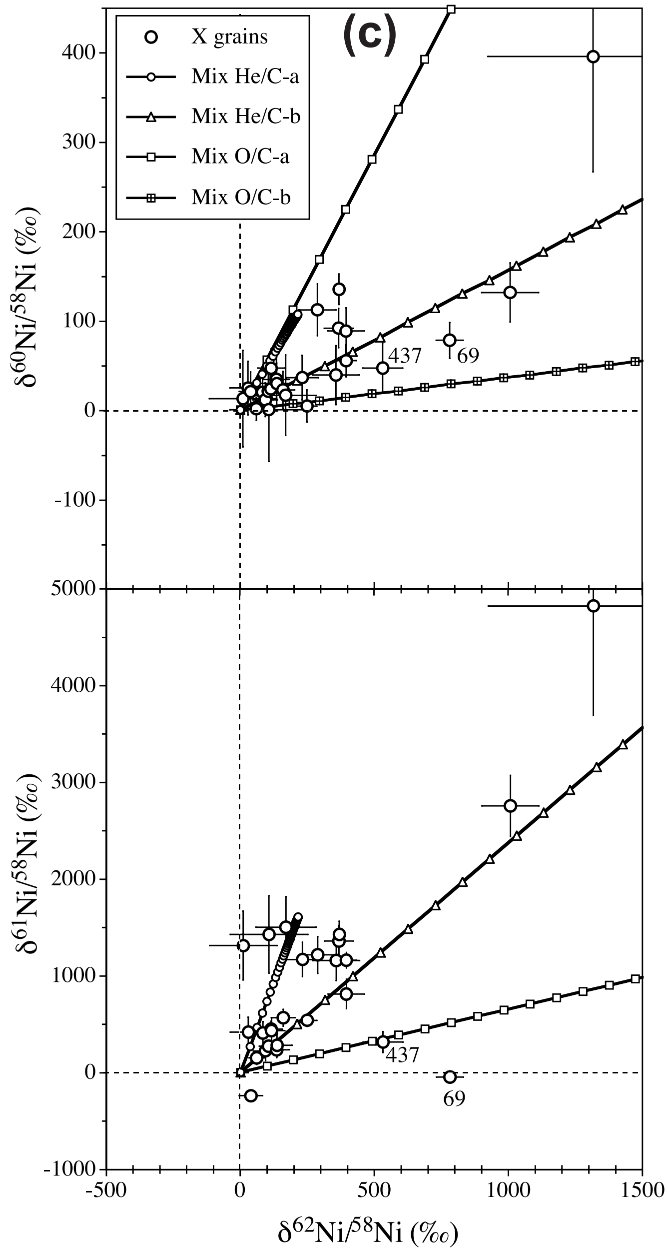

Fig. 19—*Continued*

consequence is that, if some material from these zones is admixed to material from the He/N (and He/C) zone, the corrections for ^{54}Cr and ^{58}Fe become much larger. This would result in larger ^{54}Fe deficits and larger ^{60,61,62}Ni excesses than those shown in Figure 18 and Figure 19. If we scale the ^{54}Cr/^{52}Cr and ^{58}Fe/^{56}Fe ratios with the observed ^{57}Fe/^{56}Fe (or ^{61}Ni/^{58}Ni) ratios, the ^{54}Cr and ^{58}Fe corrections in a few cases exceed the signals at mass 54 and mass 58. We have already shown that the Fe and Ni isotopic ratios of most X grains are incompatible with admixtures from the O/C zone large enough to account for the observed ^{62}Ni excesses. The problems with the ^{54}Cr and ^{58}Fe corrections make this situation even worse, and thus provide additional evidence against any substantial contributions from the O/C zone.

4.2.1.4. Dependence of Mixing Models on SN Mass and Neutron Capture Cross Sections

For the comparison of the Fe and Ni isotopic data we so far used the 25 $M_{\odot}$ model by Rauscher et al. (2002). In order to see how much the model predictions depend on the mass of the SN we also performed mixing calculations for the 15 $M_{\odot}$ model. For the Fe isotopic ratios the results are very similar to those obtained with the 25 $M_{\odot}$ model. For mixing of material from the He/N zone with material from different layers of the He/C zone and material from the O/C zone we again obtain mixing lines that, in a Fe three-isotope plot such as that in Figure 16*a*, are close to the *y*-axis. These mixing lines cover the data for grains with ^{57}Fe excesses quite well. Similar to the 25 $M_{\odot}$ SN model (Fig. 16*a*), lines resulting from mixing between He/N and Ni-core material cover a range in (negative) slopes depending on varying assumptions of Co/Fe fractionation and grain formation time; however, most of these lines miss the grain data. Also, since the Ni isotopic ratio data seem to exclude any substantial contributions from the Ni core, we do not display the results of mixing calculations for the Fe isotopes.

For the Ni isotopic ratios the results of mixing for a 15 $M_{\odot}$ SN model are shown in Figure 19*b* and compared to the data for

X grains. Similar to the ^{58}Fe corrections we applied to the ^{58}Ni signals in Figure 19*a*, we also scaled the $^{58}Fe/^{56}Fe$ ratios predicted for the 15 $M_\odot$ model with the $^{57}Fe/^{56}Fe$ ratios measured in the individual grains. In contrast to Figure 19*a*, only the Ni ratios corrected in this way are plotted in Figure 19*b*. As can be seen, the mixing lines are somewhat steeper for the 15 $M_\odot$ model than for the 25 $M_\odot$ model and, for the mixes with the He/C zone, appear to cover the grain data slightly better. Again, the mixing lines for mixing with material from the O/C zone and the Ni core in the lower panel ($\delta^{61}Ni/^{58}Ni$ vs. $\delta^{62}Ni/^{58}Ni$) miss most of the grain data and this mismatch excludes substantial contributions from these zones.

The Rauscher et al. (2002) SN models used the nuclear cross sections given by Bao et al. (2000). Recently, new determinations of the ^{60}Ni and ^{62}Ni neutron-capture cross sections have been made (Corvi et al. 2002; Nassar et al. 2005; Alpizar-Vicente et al. 2008). The most important change has been an increase of the ^{62}Ni capture cross section by almost a factor of 2. The Fe and Ni isotopes in the He/C, O/C, and O/Ne zones are affected by neutron capture, and the large abundances of ^{57}Fe, ^{58}Fe, ^{61}Ni, and ^{62}Ni found in these zones (see Fig. 15) are due to the weak *s*-process. An increase of the ^{62}Ni *n*-capture cross section will result in a reduction in the ^{62}Ni abundance. While we still have to await the results of full-blown SN models, we can estimate the expected ^{62}Ni abundance in the layers that experienced neutron capture. Following the suggestion of Woosley & Weaver (1995), we used the ^{54}Fe abundance in these zones to obtain an estimate of the total neutron exposure suffered by a given layer. Since the *s*-process does not feed ^{54}Fe, which thus behaves like a *p*-process nuclide, this isotope (as well as ^{56}Fe and ^{58}Ni) is destroyed by neutron capture (see Fig. 15). With the total neutron exposure derived from the ^{54}Fe abundance relative to the original abundance (still preserved in the H envelope and the He/N zone; see Fig. 15), we calculated the expected ^{62}Ni abundances. We obtain abundances that are 94% in the outer He/C zone, 72% in the inner He/C zone, and 63% in the outer O/C zone relative to those in the 25 $M_\odot$ SN models calculated with the Bao et al. (2000) cross sections. The resulting mixing curves are shown in Figure 19*c*. Since the expected ^{62}Ni abundances are smaller than in the original model, the mixing lines are steeper than those for the model with the old cross sections (Fig. 19*a*), as can be seen by comparing the two figures. Similarly, the mixing lines for the 15 $M_\odot$ model with the new cross sections would be steeper than those in Figure 19*b*. However, for the He/N-He/C mix all these cases would cover most of the grain data fairly well if we adjust the position (i.e., interior mass) of the chosen He/C layer and the mixing ratio for individual grains. In all cases, the He/N-O/C mixing lines miss most of the grain data in the $\delta^{61}Ni/^{58}Ni$ versus $\delta^{62}Ni/^{58}Ni$ three-isotope plot (bottom panels in Figs. 19*b* and 19*c*). Since the Ni isotopes in the Ni core are produced by NSE or QSE burning, the Ni isotopic ratios in this zone are not affected by the neutron-capture cross sections.

4.2.1.5. The Problem of the Missing ^{54}Fe

It has long been realized that the Si isotopic compositions of X grains require a contribution from the Si/S zone, where the Si consists mostly of ^{28}Si (see Fig. 17). However, as can be seen, this zone is also rich in ^{54}Fe. Admixture of only 1‰ of material from the Si/S zone at 2.35 $M_\odot$ (Fig. 17) to a mixture of He/N and He/C material that reproduces the Fe and Ni isotopic ratios of most X grains fairly well gives $\delta^{29}Si/^{28}Si = -344‰$ and $\delta^{30}Si/^{28}Si = -303‰$ and an admixture of 2‰ gives $\delta^{29}Si/^{28}Si = -541‰$ and $\delta^{30}Si/^{28}Si = -514‰$. However, these admixtures also result in large ^{54}Fe excesses with $\delta^{54}Fe/^{56}Fe = 664‰$ and $\delta^{54}Fe/^{56}Fe = 1354‰$, respectively. We can reduce the contribution of ^{54}Fe by moving a little outward in the Si/S zone. A 3‰ admixture of a layer at 2.5 $M_\odot$ interior mass to our He/N-He/C mix yields $\delta^{29}Si/^{28}Si = -543‰$ and $\delta^{30}Si/^{28}Si = -509‰$, but only $\delta^{54}Fe/^{56}Fe = 53‰$. Another possible mechanism to avoid large ^{54}Fe excesses in X grains is elemental fractionation between Si and Fe. In this scenario only Si from the Si/S zone made it into the mix from which the X grains condensed, but it was not accompanied by the large amount of ^{54}Fe from this zone.

Neither alternative is very appealing. The first consists of fine-tuning SN mixing in order to reproduce the grain's isotopic compositions, while the second consists of invoking a chemical process we really do not understand. As was discussed in connection with the Fe, Co, and Ni elemental distributions within the grains, there is plenty of evidence for elemental fractionation in X grains. Fractionation can certainly occur during grain formation, when different trace elements condense into SiC in varying degrees, according to volatility. In addition, the preferential ability of some elements to form compounds such as carbides, which can fit into the SiC crystal structure, is an important consideration. Another possible mechanism of elemental fractionation is the inclusion of subgrains. We have seen that X grains contain Fe-rich subgrains whose Ni/Fe ratios are quite different from the Ni/Fe ratio in the rest of the grain. In some cases, these subgrains have different Fe isotopic ratios from each other and from the rest of the SiC grain. Thus these subgrains must have condensed in reservoirs of the same supernova that are different from the reservoir in which the SiC grains condensed. Transmission electron microscope investigations of X grains (Stroud et al. 2004; Hynes et al. 2006b) have shown that the grains appear to consist of aggregates of smaller units, implying rapid grain growth. These subunits probably condensed independently, although they were temporally contiguous, and were later welded together. Thus it is conceivable that the ^{28}Si from the Si/S zone was separated from the ^{54}Fe in this layer by condensation into different compounds. This is not a well-understood field, and it is made more difficult by the fact that the elemental compositions of different SN layers are very different from the solar composition. We can only hope that future studies of condensation in such extremely nonsolar gases will shed light on the possible physical separation of different elements in SN ejecta.

4.2.1.6. The Problem of Grains with ^{57}Fe Deficits

While the ^{57}Fe and $^{60,61,62}Ni$ excesses in X grains can be reasonably well understood in the framework of SN models, we are at a loss to explain the ^{57}Fe deficits seen in several grains. The only zones where ^{57}Fe is depleted are at mass 2.1 $M_\odot$ in the Ni core, where ^{57}Fe drops sharply and ^{54}Fe rises rapidly and around mass 2.8 $M_\odot$ in the O/Si zone (Fig. 17). We mixed material from each of these layers with either material from the He/N zone or with a mix of He/N and He/C material. In each case we encountered serious problems with other isotopic ratios. By mixing about 1% from the core layer at mass 2.1 $M_\odot$ to He/N material we obtain $\delta^{57}Fe/^{56}Fe = -480‰$ and $\delta^{54}Fe/^{56}Fe = -24‰$. As an additional benefit, we obtain $^{29,30}Si$ depletions of about 480‰. However, we also obtain depletions in $^{60,61,62}Ni$ of 550‰, which are not seen in the grains (Fig. 6*b*). The reason is that in this core layer the abundances of these three Ni isotopes have dropped to almost zero (Fig. 17). Adding almost pure ^{58}Ni reduces the $^{60,61,62}Ni/^{58}Ni$ ratios to somewhat less than half their solar values. The situation is not any better with the O/Si zone around mass 2.8 $M_\odot$. Although $\delta^{57}Fe/^{56}Fe = -700‰$ in this layer, there is simply too little Fe to change the isotopic compositions of He/N and He/C material to a ^{57}Fe-depleted composition without serious

TABLE 3

Model Predictions for the Fe and Ni Isotopic Ratios in the Envelopes of AGB Stars

Mass	Z	$\delta^{54}Fe/^{56}Fe$ (‰)	$\delta^{57}Fe/^{56}Fe$ (‰)	$\delta^{60}Ni/^{58}Ni$ (‰)	$\delta^{60}Ni/^{58}Ni$[a] (‰)	$\delta^{60}Ni/^{58}Ni$[b] (‰)	$\delta^{61}Ni/^{58}Ni$ (‰)	$\delta^{61}Ni/^{58}Ni$[b] (‰)	$\delta^{62}Ni/^{58}Ni$ (‰)	$\delta^{62}Ni/^{58}Ni$[b] (‰)
1.5	0.02	−3	42	10	10	13	125	109	101	64
	0.01	−4	67	13	13	16	163	137	101	61
	0.006	−9	142	26	27	33	320	271	161	98
	0.003	−25	357	118	139	...	1173	...	825	...
2	0.02	−4	60	14	15	...	181	...	148	...
	0.01	−8	126	25	26	...	315	...	203	...
	0.006	−17	247	57	65	...	645	...	400	...
	0.003	−37	528	149	184	...	1568	...	1030	...
3	0.02	−7	97	25	27	32	293	268	243	150
	0.01	−11	161	38	42	47	434	402	305	189
	0.006	−16	206	138	238	249	1262	1278	1167	701
	0.003	−14	162	554	2123	...	6396	...	7938	...

Notes.—Shown are the compositions after the third dredge-up following the last thermal pulse. It is assumed that the parent stars have solar initial isotopic compositions.

[a] Includes the decay of ^{60}Fe.

[b] Calculated with the new ^{60}Ni and ^{62}Ni neutron capture cross sections (Corvi et al. 2002; Alpizar-Vicente et al. 2008).

unpleasant consequences. Admixture of 20% of O/Si material yields only $\delta^{57}Fe/^{56}Fe = -25‰$ while producing huge excesses in ^{60}Ni and ^{62}Ni ($\delta^{60}Ni/^{58}Ni = 5{,}140‰$, $\delta^{62}Ni/^{58}Ni = 24{,}200‰$). In addition, the high O abundance from this layer results in a O/C ratio of ~300, not conducive to the condensation of SiC. Thus, it does not appear to be possible to explain the ^{57}Fe deficiencies observed in several grains by the predicted compositions in zones of a given supernova.

The range of Si and Ti isotopic ratios observed in mainstream, Y, and Z SiC grains have been interpreted not to be the result of nucleosynthesis in a given stellar source, but to reflect the initial compositions of the grains' parent stars. These initial compositions have in turn been related to the Galactic evolution of these isotopes, indicating that stars with different metallicities contributed SiC grains to the solar system (see, e.g., Timmes & Clayton 1996; Hoppe et al. 1997; Alexander & Nittler 1999; Lugaro et al. 1999; Nittler & Alexander 2003; Zinner et al. 2006b, 2007). We therefore investigated whether Galactic evolution of the Fe isotopes could explain deficits in ^{57}Fe. From the total yields of Fe isotopes calculated from Chandrasekhar-mass (Nomoto et al. 1997) and sub-Chandrasekhar-mass (Woosley & Weaver 1994) models of Type Ia supernovae and from core-collapse (Type II) supernovae (Woosley & Weaver 1995; Nomoto et al. 1997; Rauscher et al. 2002) we calculated $^{54}Fe/^{56}Fe$ and $^{57}Fe/^{56}Fe$ ratios. Unfortunately, these models do not offer much hope for explaining the ^{57}Fe deficits in some grains as the effect of Galactic evolution, since essentially all of the models exhibit ^{57}Fe excesses. The only exceptions are the 20 $M_\odot$ models of subsolar metallicities $Z = 0.1\ Z_\odot$ ($\delta^{57}Fe/^{56}Fe = -282‰$) and $Z = 0.01\ Z_\odot$ ($\delta^{57}Fe/^{56}Fe = -580‰$) by Woosley & Weaver (1995). However, these two models predict even larger ^{54}Fe deficits ($\delta^{54}Fe/^{56}Fe = -674‰$ and $-704‰$, respectively) than seen in the grains. In general, ^{54}Fe deficits are quite common among these models. The sub-Chandrasekhar-mass Type Ia models have large ^{54}Fe deficits, as have all Type II SN models with subsolar metallicity (Woosley & Weaver 1995). Thus, the $^{54}Fe/^{56}Fe$ ratio must have undergone large changes during Galactic evolution. Early Type II supernovae of low metallicity produced low $^{54}Fe/^{56}Fe$ ratios, and even the integrated output of Type II supernovae of solar metallicity results in a ^{54}Fe deficit (Nomoto et al. 1997). It is only with late contributions from Chandrasekhar-mass Type Ia supernovae, which overproduce ^{54}Fe, that the $^{54}Fe/^{56}Fe$ ratio reached the solar value. Such an evolution did not take place for the $^{57}Fe/^{56}Fe$ ratio. Apparently, the production of ^{56}Fe and ^{57}Fe (as their precursors ^{56}Ni and ^{57}Ni) by NSE nucleosynthesis is so similar that all different types of supernovae produce these two isotopes in similar proportions. Figure 17 clearly shows that the distribution of ^{56}Fe and ^{57}Fe in the inner zones is quite different from that of ^{54}Fe. The first two isotopes are most abundant in the zone where Si has burned completely, whereas ^{54}Fe is destroyed in this zone but is abundant in the region where Si had burned incompletely. Contributions from AGB stars also affected the Galactic chemical evolution in the late stage of Galactic history. However, the effect on the evolution of the Fe isotopes is probably minor. AGB stars produce ^{57}Fe excesses and ^{54}Fe deficits. The first do not help in explaining ^{57}Fe deficits observed in grains; the ^{54}Fe deficits in AGB stars are small (see Table 3) and cannot offset the large ^{54}Fe contributions from Type Ia supernovae.

4.2.1.7. Iron Implantation in Presolar Supernova Grains?

Clayton et al. (2002) proposed that SiC grains of type X originally condensed from material in the Si-rich Si/S zone (see Fig. 17), but that later these grains moved through the reverse shocked gas of overlying layers, and that elements from these layers, among them Fe, were implanted. Our present study, as well as previous ones, do not support this proposal. First, the X grains contain Fe-rich subgrains, which in some cases have different Fe isotopic compositions. These subgrains apparently existed as separate grains and were included into the condensing SiC grains. Alternatively, they accreted together with smaller SiC grains and were then fused into the larger X grains we now analyze in the laboratory. Second, most of the Fe and Ni in the grains comes from zones that have close-to-solar isotopic compositions, implying that the Fe/Co/Ni ratios in these zones are approximately solar. We observe large excesses of Co and Ni over Fe in most grains (see Figs. 7*a* and 7*b*). Implantation from a gas would not distinguish between different elements and thus could not result in large fractionation between these elements. Fractionation is also observed for other elements. For example, Mg in X grains is even more depleted than Fe, whereas Al contents are quite high. Clayton et al. (2002) also proposed that ^{26}Al was implanted into X grains. If this were the case, corresponding large amounts of Mg would also been implanted, which is not observed. Finally, Clayton et al. (2002) calculate

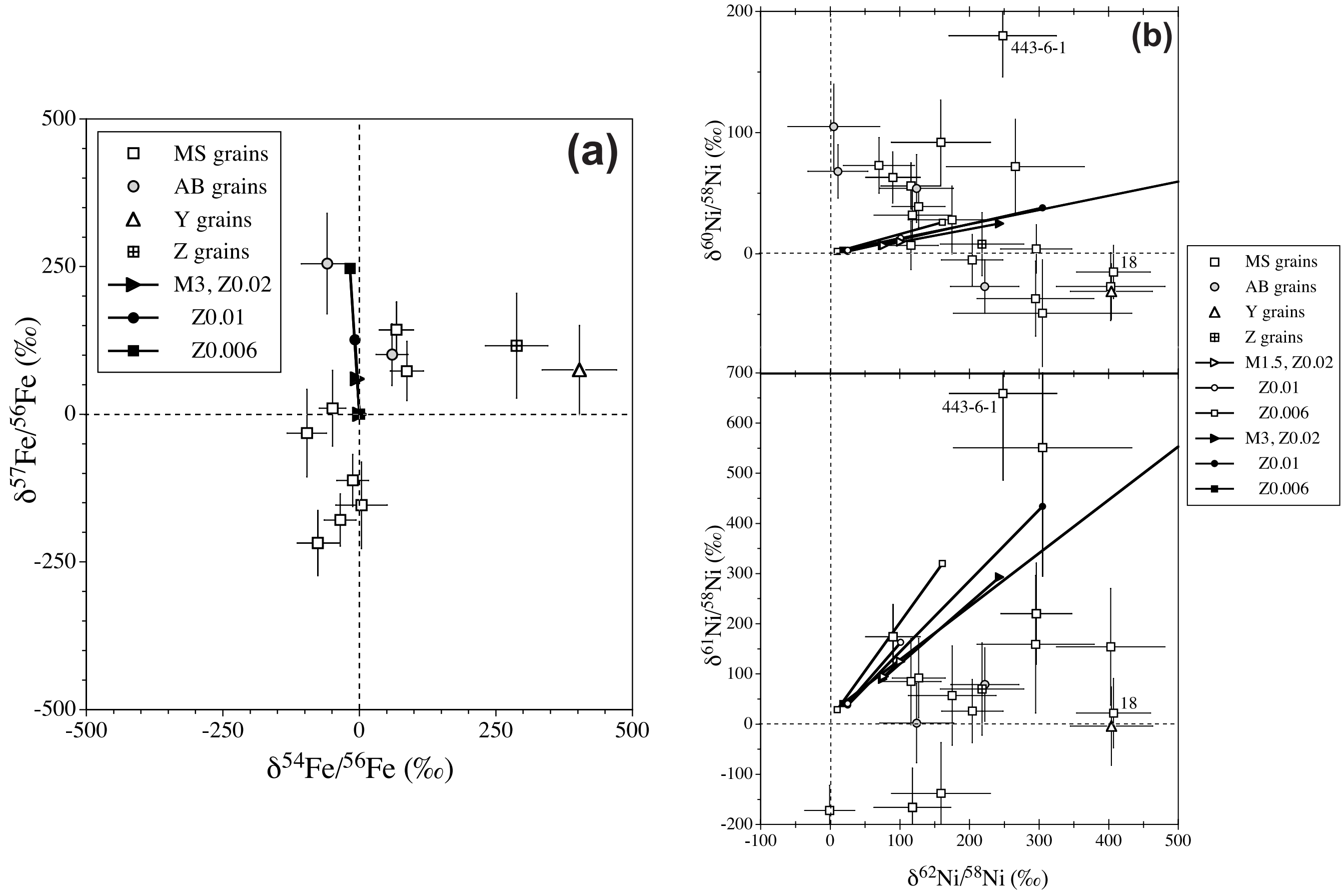

FIG. 20.—(*a*) Fe isotopic ratios in mainstream, AB, Y, and Z grains are compared with AGB model predictions in a 3 $M_\odot$ star with a range of metallicities. The model predictions show the isotopic ratios (essentially normal) at the time the stars become carbon stars, and after the third dredge-up following the last thermal pulse. (*b*) and (*c*) Ni isotopic compositions in mainstream, AB, Y, and Z grains are compared with model predictions in 1.5 and 3 $M_\odot$ stars with different metallicities. In (*b*), the neutron capture cross sections by Bao et al. (2000) are used in the models; in (*c*), the recently determined cross sections for ^{60}Ni (Corvi et al. 2002) and ^{62}Ni (Alpizar-Vicente et al. 2008) are used.

an implantation depth of up to 0.1 μm. While concentrations of Fe, Co, and Ni might vary inside of X grains, it is clear from the depth profiles in Figures 9–13 that these elements are not confined to the surfaces of the grains, which, on average, are 2.5 μm in size. Thus, there is plenty of evidence that trace elements either condensed into the SiC X grains or were included as subgrains, but were not implanted.

4.2.2. *Grains from AGB Stars of Low-to-Intermediate Mass*

The Fe and Ni isotopic compositions of many of the other SiC grain types are no less puzzling than those of some of the X grains. Most of the mainstream and AB grains have solar isotopic ratios (Table 2) and are not plotted in Figures 4–6. Mainstream, Y, and Z grains are believed to have an origin in C-rich AGB stars, the mainstream grains in stars of close-to-solar metallicity, and Y and Z grains from stars of lower-than-solar metallicity. In the thermally pulsing phase of these stars, the capture of neutrons in the He intershell, either from the ^{13}C$(\alpha,n)^{16}$O or ^{22}Ne$(\alpha,n)^{25}$Mg neutron sources (e.g., Busso et al. 1999; Herwig 2005) leads to destruction of ^{54}Fe and ^{58}Ni and production of ^{57}Fe, ^{60}Fe, ^{61}Ni, and ^{62}Ni. Each thermal pulse (TP) is followed by the so-called third dredge-up (TDU), which mixes newly processed material from the He intershell into the star's envelope. Table 3 gives predicted Fe and Ni isotopic ratios in the envelope of AGB stars of different masses and metallicities at the time after the last thermal pulse and the subsequent third-dredge-up episode. Since the amount of ^{13}C in the intershell cannot be derived from first principles, a free parameter, the strength of the so-called ^{13}C pocket, is used (Gallino et al. 1998). The δ-values given in Table 3 are obtained with the standard (ST) ^{13}C pocket. Recent measurements of Mo, Zr, and Ba isotopic ratios in individual mainstream grains constrain the ^{13}C pocket to values close to the ST case (Barzyk et al. 2007; Marhas et al. 2007c). The isotopic ratios are given for models using the neutron capture cross sections of Bao et al. (2000). We also include model predictions calculated with the new cross sections for ^{60}Ni (Corvi et al. 2002) and ^{62}Ni (Alpizar-Vicente et al. 2008). In particular, the cross sections for ^{62}Ni have been found to be much higher than those given by Bao et al. (2000), resulting in smaller predicted ^{62}Ni excesses (see Table 3).

As has been mentioned above, the range of Si and Ti isotopic ratios of SiC grains from AGB stars is determined by both nucleosynthesis in the parent stars and Galactic evolution of the isotopes. This is most likely also the case for the Fe and Ni isotopic ratios. The predictions shown in Table 3 assume that the initial isotopic compositions of the parent stars are solar. This is most likely not the case, and the δ-values given in the table should be considered shifts from the original isotopic ratios. Let us look first at the Fe isotopic ratios. Figure 20*a* shows the Fe isotopic ratios of mainstream, AB, Y, and Z grains together with predictions for 3 $M_\odot$ stars with a range of metallicities. AGB models predict small ^{54}Fe deficits and larger ^{57}Fe excesses in stars

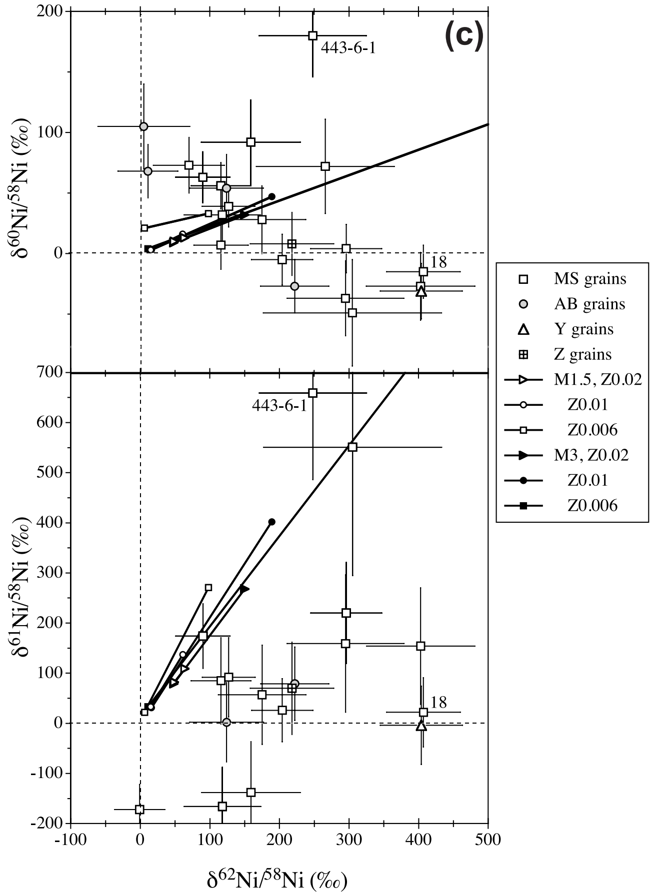

FIG. 20—*Continued*

of solar metallicity ($Z = 0.02$). These effects are larger in low-metallicity AGB stars. The ^{57}Fe excesses in two mainstream grains are within the range expected for stars of solar and half-solar metallicity. Their ^{54}Fe excesses and the ^{54}Fe deficits in the two grains with normal ^{57}Fe/^{56}Fe ratios might be explained by Galactic evolution of the ^{54}Fe/^{56}Fe ratio. However, the ^{57}Fe deficits in several mainstream grains (Fig. 4) pose the same problem as those in X grains. As discussed in connection with those X grains, SN models indicate that the ^{57}Fe/^{56}Fe ratio is not expected to undergo any strong Galactic evolution. The ^{57}Fe deficits in X and mainstream grains thus remain a puzzle. Another puzzle is presented by the ^{54}Fe excesses measured in a Y and a Z grain (Fig. 20*a*). These grain types are believed to originate from stars of lower-than-solar metallicity, and we expect low-metallicity stars to have ^{54}Fe deficits rather than excesses. For the Y grain, the correction for ^{54}Cr is unusually large (73%). Thus, some of the excess could possibly be due to undercorrection. However, in order to obtain a normal ^{54}Fe/^{56}Fe ratio, ^{54}Cr/^{52}Cr would have to be increased over the solar ratio by 550‰. This is unlikely in view of the fact that in this grain δ^{57}Fe/^{56}Fe = 75‰ ± 75‰. For $Z = Z_{\odot}/2$, typical for Y grains (Zinner et al. 2006b) and AGB stars of masses 1.5–3 $M_{\odot}$, the predicted ^{54}Cr excesses are between 1.3 and 1.5 times the predicted ^{57}Fe excesses (Table 3), which would result in a ^{54}Cr excess of only 100‰. The ^{54}Cr correction is only 3.5% for the Z grain and thus we definitely can exclude undercorrection for ^{54}Cr as the cause for the ^{54}Fe excess in this grain.

Moving on to the Ni isotopes (Figs. 20*b* and 20*c*), we notice that isotopic shifts due to neutron capture in AGB stars are predicted to be highest for δ^{61}Ni/^{58}Ni, followed by δ^{62}Ni/^{58}Ni (Table 3). The lines in Figures 20*b* and 20*c* are the envelope compositions evolving between the time the star becomes a carbon star (C > O) and the time of the third dredge-up after the last thermal pulse. Only small increases are predicted for the ^{60}Ni/^{58}Ni ratio in stars of solar metallicity. Some of the grain data agree with these expectations, although some do not. A group of grains with ^{60}Ni and ^{62}Ni excesses have close to the expected δ^{60}Ni/δ^{62}Ni ratios (top panels of Figs. 20*b* and 20*c*), but the ^{60}Ni/^{58}Ni ratios of several mainstream grains, especially grain 443-6-1, are too high for their ^{60}Ni/^{58}Ni ratios, and these grains plot above the lines predicted by AGB models. Several mainstream grains, such as grain 18, and the Y and Z grains have zero or negative δ^{60}Ni/^{58}Ni values but substantial ^{62}Ni excesses. In Figures 20*b* and 20*c*, they fall below all δ^{60}Ni/^{58}Ni versus δ^{62}Ni/^{58}Ni lines corresponding to the predicted shift of AGB nucleosynthesis in stars of solar and lower-than-solar metallicity. In the case of X grains with negative δ^{60}Ni/^{58}Ni values, these values were shifted to positive δ^{60}Ni/^{58}Ni values when we applied larger ^{58}Fe corrections to these grains (see above discussion and Fig. 19). However, as none of the mainstream grains have substantial ^{57}Fe excesses, larger ^{58}Fe corrections would not be justified because we do not expect an anomalous increase in the ^{58}Fe/^{56}Fe ratio. The range of ^{61}Ni excesses in mainstream grains is close to the predicted range for AGB stars of solar metallicity (bottom panels of Figs. 20*b* and 20*c*). However, almost all of these grains plot below the predicted evolution lines. The disagreement is made even worse if we use the new ^{60}Ni and ^{62}Ni cross sections in the AGB models. Because the increased ^{62}Ni cross sections result in lower ^{62}Ni excesses in the AGB models, the $\delta^{61}Ni/^{58}Ni$ versus $\delta^{62}Ni/^{58}Ni$ lines become steeper (Fig. 20*c*, *bottom*). Not only several mainstream grains but also the Y and Z grains plot below the $\delta^{61}Ni/^{58}Ni$ versus $\delta^{62}Ni/^{58}Ni$ lines.

We next explore the possible effect of the Galactic evolution of the Ni isotopes on the initial isotopic compositions of the parent stars of mainstream, Y, and Z grains. We did not calculate a detailed Galactic evolution model for Ni. However, from the yields of models for Type Ia and Type II supernovae, it appears that the $^{60,61,62}Ni/^{58}Ni$ ratios evolve from larger to smaller values with time (or metallicity) during Galactic history before the formation of the solar system. Type II SN models for low metallicity (0.1 and 0.01 $Z_\odot$) give much larger than solar $^{60,61,62}Ni/^{58}Ni$ ratios (Woosley & Weaver 1995). Even the average of Type II SN models of solar metallicity (weighted with the Salpeter initial mass function) gives positive δ-values (Nomoto et al. 1997). Type Ia Chandrasekhar-mass SN models, on the other hand, yield much lower than solar $^{60,61,62}Ni/^{58}Ni$ ratios because of the large overproduction of ^{58}Ni in these stars (Travaglio et al. 2004). The evolution from larger to smaller ratios corresponds to trajectories from the upper right to the lower left in the graphs of Figures 20*b* and 20*c*. Lacking a detailed Galactic evolution model, which would exceed the scope of this paper, we do not know the slopes of these curves. Under the assumption that stars of solar metallicity have solar Ni isotopic ratios, the parent stars of Y and Z grains, assumed to be of lower-than-solar metallicity, are expected to have initial Ni isotopic ratios that plot to the upper right of the origin (solar ratios) in the Figure 20*b* and Figure 20*c* graphs. Since the effect of AGB nucleosynthesis is to shift these compositions even farther to the upper right (lines in these figures), the Ni isotopic ratios of the Y and Z grains cannot be satisfactorily explained by a combination of Galactic evolution and neutron-capture nucleosynthesis in AGB stars. So far, we have tacitly assumed that Galactic evolution proceeds along elemental and isotopic compositions that are a thorough mix of the contributing stellar sources. This, however, does not have to be the case, and in fact, heterogeneities in the interstellar medium have been discussed before in connection with the Si isotopic ratios of mainstream SiC grains (Lugaro et al. 1999). Other isotopic ratios in these grains, in particular those of Ti, indicate that the extent of heterogeneity is limited (Nittler 2005). Still, it is certainly possible that a single precursor star strongly influenced the isotopic compositions of the parent star of a given presolar dust grain. We might pursue this question in the future.

A few of the AB grains have isotopic anomalies in Fe and Ni (Figs. 4 and 5). Because the stellar sources of AB grains have not yet been unambiguously identified (Amari et al. 2001c), it is not possible to compare the grain data with theoretical models of their production. Amari et al. (2001c) proposed as a stellar source of some AB grains born-again AGB stars such as Sakurai's object (Asplund et al. 1997, 1999). Recently, Jadhav et al. (2008) identified graphite grains with huge Ca and Ti isotopic anomalies and considered born-again AGB stars as a possible stellar source. These stars lost essentially their entire envelope and their surface composition is expected to be dominated by He-shell material, only slightly diluted by the residual envelope. For such a composition we predict large excesses of ^{57}Fe and $^{61,62}Ni$ and smaller excesses in ^{60}Ni, much larger than the ^{57}Fe excesses observed in two AB grains (Fig. 4). Furthermore, the excesses in these two grains are not accompanied by corresponding ^{61}Ni excesses (Fig. 6*b* and Table 2). A few AB grains have excesses in ^{60}Ni and ^{62}Ni (Figs. 20*b* and 20*c*), but we do not have any explanation.

5. CONCLUSIONS

We measured Fe and Ni isotopic ratios in 39 mainstream grains, 37 X grains, 11 AB grains, two Y grains, and one Z grain from the Murchison SiC separate KJG (Amari et al. 1994). The grain type classification was based on the grains' C and Si isotopic ratios. For most grains (all X grains), we also measured the N isotopic ratios.

The Ni/Fe and Co/Fe ratios in all grain types are much higher than in the gas from which the grains are believed to have formed. At least half the X grains, as well as a couple of mainstream grains, contain subgrains that have higher Fe/Ni than the bulk of these grains and the grains without apparent subgrains.

Most X grains have Fe and Ni isotopic anomalies dominated by excesses in ^{57}Fe, ^{61}Ni, and ^{62}Ni. ^{60}Ni excesses are small and the $^{54}Fe/^{56}Fe$ ratios of almost all X grains are normal. These isotopic compositions are best explained by the mixing of material from the He/N zone of Type II supernovae with material from the He/C zone, where neutron capture resulted in ^{57}Fe and $^{60,61,62}Ni$ excesses. A puzzling result is the lack of any ^{54}Fe excesses. The Si/S zone, which must have contributed ^{28}Si in order to explain the ^{28}Si excesses in X grains, is very rich in ^{54}Fe. It remains to be seen whether elemental fractionation between Si and Fe provides an explanation for this puzzle. We cannot offer any good explanation for the ^{57}Fe deficits observed in a few X grains.

A smaller fraction of mainstream and AB grains than of X grains has anomalies. Some mainstream grains with ^{57}Fe depletions present the same problem as the X grains with ^{57}Fe depletions. The most common Ni isotopic anomalies in mainstream grains are ^{62}Ni excesses. While neutron capture in AGB stars is expected to produce such excesses, observed ^{62}Ni excesses in some grains are larger than predicted for AGB stars of solar metallicity, and are not accompanied by corresponding ^{61}Ni excesses. One Y grain and one Z grain have excesses in ^{54}Fe and ^{62}Ni, but close to normal $^{57}Fe/^{56}Fe$ and $^{60.61}Ni/^{58}Ni$ ratios. These signatures are not expected for grains from low-metallicity AGB stars, but we still have to explore in more detail the Galactic evolution of the Fe and Ni isotopes.

The results obtained in this study present new challenges to our understanding of nucleosynthetic processes in supernovae and low-mass AGB stars. They also point to future efforts we plan to undertake to improve this understanding. One is to investigate the large elemental fractionation among Fe, Co, and Ni observed in the grains. Another is to study possible elemental fractionation of Si and Fe from the Si/S zone before the formation of X grains. Such fractionation would explain why X grains show large ^{28}Si excesses without having large excesses in ^{54}Fe, which according to SN models is abundant in the Si/S zone. Finally, we plan to investigate the Galactic evolution of the Fe and Ni isotopes in detail. For this we will try to measure Fe and Ni isotopic ratios in Z grains. Isotopic signatures interpreted to be due to Galactic evolution can clearly be seen in Si and Ti (e.g., Zinner et al. 2006b, 2007). However, such measurements are not a trivial undertaking. The abundance of Z grains among KJG grains is less than 1% but increases to more than 5% for sub-μm grains (Zinner et al. 2007). While it is easier to locate Z grains among small SiC grains, it remains to be seen whether they contain enough Fe and Ni for meaningful isotopic analysis.

We thank Frank Stadermann for his help in all matters related to the NanoSIMS and Tim Smolar for keeping the instrument functioning. We are grateful to Roy Lewis for providing the KJG grain mounts. We also appreciate discussions with Marco Pignatari and the help of Andy Davis in providing some of the Fe and Ni data tables of AGB models. The paper has benefited from the comments by a reviewer. This work has been supported by NASA fund NNG 05GF81G (E.Z. PI) and by the Italian MIUR-PRIN06 project 2006022731-005 (R.G.).

REFERENCES

Alexander, C. M. O'D., & Nittler, L. R. 1999, ApJ, 519, 222
Alpizar-Vicente, A. M., et al. 2008, Phys. Rev. C, 77, 015806
Amari, S., Gao, X., Nittler, L. R., Zinner, E., José, J., Hernanz, M., & Lewis, R. S. 2001a, ApJ, 551, 1065
Amari, S., Hoppe, P., Zinner, E., & Lewis, R. S. 1995, Meteoritics, 30, 679
Amari, S., Lewis, R. S., & Anders, E. 1994, Geochim. Cosmochim. Acta, 58, 459
Amari, S., Nittler, L. R., Zinner, E., Gallino, R., Lugaro, M., & Lewis, R. S. 2001b, ApJ, 546, 248
Amari, S., Nittler, L. R., Zinner, E., Lodders, K., & Lewis, R. S. 2001c, ApJ, 559, 463
Anders, E., & Grevesse, N. 1989, Geochim. Cosmochim. Acta, 53, 197
Asplund, M., Gustafsson, B., Lambert, D. L., & Rao Kameswara, N. 1997, A&A, 321, L17
Asplund, M., Lambert, D. L., Kipper, T., Pollacco, D., & Shetrone, M. D. 1999, A&A, 343, 507
Bao, Z. Y., Beer, H., Käppeler, F., Voss, F., Wisshak, K., & Rauscher, T. 2000, At. Data Nucl. Data Tables, 76, 70
Barzyk, J. G., et al. 2007, Meteoritics Planet. Sci., 42, 1103
Bernatowicz, T. J., & Zinner, E., 1997, in AIP Conf. Proc. 402, Astrophysical Implications of the Laboratory Study of Presolar Materials (New York: AIP), 750
Busso, M., Gallino, R., & Wasserburg, G. J. 1999, ARA&A, 37, 239
Clayton, D. D., Meyer, B. S., The, L.-S., & El Eid, M. F. 2002, ApJ, 578, L83
Clayton, D. D., & Nittler, L. R. 2004, ARA&A, 42, 39
Corvi, F., Fioni, G., Gunsing, F., Mutti, P., & Zanini, L. 2002, Nucl. Phys. A, 697, 581
Gallino, R., Arlandini, C., Busso, M., Lugaro, M., Travaglio, C., Straniero, O., Chieffi, A., & Limongi, M. 1998, ApJ, 497, 388
Gyngard, F., Amari, S., Jadhav, M., Marhas, K., Zinner, E., & Lewis, R. S. 2006, Meteoritics Planet. Sci., 41, A71
Heil, M., Käppeler, F., Uberseder, E., Gallino, R., & Pignatari, M. 2008, Phys. Rev. C, 77, 015808
Herwig, F. 2005, ARA&A, 43, 435
Hinton, R. W. 1990, Chem. Geol., 83, 11
Hoppe, P., Amari, S., Zinner, E., Ireland, T., & Lewis, R. S. 1994, ApJ, 430, 870
Hoppe, P., Annen, P., Strebel, R., Eberhardt, P., Gallino, R., Lugaro, M., Amari, S., & Lewis, R. S. 1997, ApJ, 487, L101
Hoppe, P., & Besmehn, A. 2002, ApJ, 576, L69
Hoppe, P., Eberhardt, P., Amari, S., & Lewis, R. S. 1998, Lunar Planet. Sci. XXIX, ed. D. Blanchard & D. Black (Houston: LPI), abstract 1126
Hoppe, P., & Ott, U. 1997, in Astrophysical Implications of the Laboratory Study of Presolar Materials, ed. T. J. Bernatowicz & E. Zinner (New York: AIP), 27
Hoppe, P., Strebel, R., Eberhardt, P., Amari, S., & Lewis, R. S. 1996, Science, 272, 1314
———. 2000, Meteoritics Planet. Sci., 35, 1157
Hynes, K. M., Croat, T. K., Amari, S., Mertz, A. F., & Bernatowicz, T. J. 2006a, Meteoritics Planet. Sci., 41, A83
———. 2006b, Lunar Planet. Sci. XXXVII, ed. S. J Mackwell (Houston: LPI), abstract 2202
Jadhav, M., Amari, S., Marhas, K. K., Zinner, E., Maruoka, T., & Gallino, R. 2008, ApJ, 682, 1479
Kane, J. S. 1998, Geostandards Newsletter: J. Geostandards & Geoanal., 22, 7
Kashiv, Y., Cai, Z., Lai, B., Sutton, S. R., Lewis, R. S., Davis, A. M., & Clayton, R. N. 2001, Lunar Planet. Sci. XXXII, ed. C. B. Agee & D. Black (Houston: LPI), abstract 2192
Kashiv, Y., Cai, Z., Lai, B., Sutton, S. R., Lewis, R. S., Davis, A. M., Clayton, R. N., & Pellin, M. J. 2002, Lunar Planet. Sci. XXXIII, ed. C. B. Agee & D. Black (Houston: LPI), abstract 2056
Knight, K., et al. 2008, Lunar Planet. Sci. XXXIX, ed. S. J. Mackwell (League City: LPI), abstract 2135
Lin, Y., Amari, S., & Pravdivtseva, O. 2002, ApJ, 575, 257
Lodders, K., & Amari, S. 2005, Chem. Erde, 65, 93
Lodders, K., & Fegley, B., Jr. 1995, Meteoritics, 30, 661
Lugaro, M., Davis, A. M., Gallino, R., Pellin, M. J., Straniero, O., & Käppeler, F. 2003, ApJ, 593, 486
Lugaro, M., Zinner, E., Gallino, R., & Amari, S. 1999, ApJ, 527, 369
Marhas, K. K., Amari, S., Gyngard, F., & Zinner, E. 2007a, Meteoritics Planet. Sci., 42, A97
Marhas, K. K., Amari, S., Gyngard, F., Zinner, E., & Lewis, R. S. 2007b, Lunar Planet. Sci. XXXVIII, ed. S. J. Mackwell (League City: LPI), abstract 2124
Marhas, K. K., Hoppe, P., & Besmehn, A. 2004, Lunar Planet. Sci. XXXV, ed. S. J. Mackwell (Houston: LPI), abstract 1834
Marhas, K. K., Hoppe, P., & Ott, U. 2007c, Meteoritics Planet. Sci., 42, 1077
Meyer, B. S., Weaver, T. A., & Woosley, S. E. 1995, Meteoritics, 30, 325
Meyer, B. S., & Zinner, E. 2006, in Meteorites and the Early Solar System II, ed. D. S. Lauretta & H. Y. McSween, Jr. (Tucson: Univ. Arizona), 69
Nassar, H., et al. 2005, Phys. Rev. Lett., 94, 092504
Nittler, L. R. 2003, Earth Planet. Sci. Lett., 209, 259
———. 2005, ApJ, 618, 281
Nittler, L. R., & Alexander, C. M. O'D. 2003, Geochim. Cosmochim. Acta, 67, 4961
Nittler, L. R., Amari, S., Zinner, E., Woosley, S. E., & Lewis, R. S. 1996, ApJ, 462, L31
Nittler, L. R., & Hoppe, P. 2005, ApJ, 631, L89
Nittler, L. R., et al. 1995, ApJ, 453, L25
Nomoto, K., Iwamoto, K., Nakasato, N., Thielemann, F.-K., Brachwitz, F., Tsujimoto, T., Kubo, Y., & Kishimoto, N. 1997, Nucl. Phys. A, 621, 467
Owen, T., Mahaffy, P. R., Niemann, H. B., Atreya, S., & Wong, M. 2001, ApJ, 553, L77
Pignatari, M., Gallino, R., Baldovin, C., Wiescher, M., Herwig, F., Heger, A., Heil, M., & Käppeler, F. 2006, Proc. Int. Symp. Nucl. Astrophysics, Nuclei in the Cosmos IX, ed. A. Mengori (Trieste: Proc. Sci.), 61.1
Rauscher, T., Heger, A., Hoffman, R. D., & Woosley, S. E. 2002, ApJ, 576, 323
Rocholl, A. B. E., et al. 1997, Geostandards Newsletter: J. Geostandards & Geoanal., 21, 101
Slodzian, G. 2003, Applied Surface Sci., 203, 798
Stadermann, F. J., Walker, R. M., & Zinner, E. 1999a, Meteoritics Planet. Sci., 34, A111
———. 1999b, Lunar Planet. Sci. XXX, ed. C. Agee & D. Black (Houston: LPI), abstract 1407
Stroud, R. M., Nittler, L. R., & Hoppe, P. 2004, Meteoritics Planet. Sci., 39, A101
The, L.-S., El Eid, M. F., & Meyer, B. S. 2000, ApJ, 533, 998
———. 2007, ApJ, 655, 1058
Timmes, F. X., & Clayton, D. D. 1996, ApJ, 472, 723
Travaglio, C., Hillebrandt, W., Reinecke, M., & Thielemann, F.-K. 2004, A&A, 425, 1029
Virag, A., Wopenka, B., Amari, S., Zinner, E., Anders, E., & Lewis, R. S. 1992, Geochim. Cosmochim. Acta, 56, 1715
Woosley, S. E., & Weaver, T. A. 1994, ApJ, 423, 371
———. 1995, ApJS, 101, 181
Yoshida, T., & Hashimoto, M. 2004, ApJ, 606, 592
Zinner, E. 1998, Ann. Rev. Earth Planet. Sci., 26, 147
———. 2007, in Treatise on Geochemistry Update, ed. H. D. Holland, K. K. Turekian & A. Davis (Oxford: Elsevier), 1.02, http://www.sciencedirect.com/science/referenceworks/9780080437514
Zinner, E., Nittler, L. R., Alexander, C. M. O'D., & Gallino, R. 2006a, NewA Rev., 50, 574
Zinner, E., Nittler, L. R., Gallino, R., Karakas, A. I., Lugaro, M., Straniero, O., & Lattanzio, J. C. 2006b, ApJ, 650, 350
Zinner, E., et al. 2007, Geochem. Cosmochim. Acta, 71, 4786